NTNU

Norwegian University of
Science and Technology

Modelling of Wave Propagation in Shallow Water Environment

Skjalg Andersson

Master of Science in Electronics
Submission date: June 2008
Supervisor: Hefeng Dong, IET
Co-supervisor: Svein Arne Frivik, Western Geco

Norwegian University of Science and Technology
Department of Electronics and Telecommunications

Problem Description

Use raytracing to model wave propagation in a shallow water environment with a varying geometry (dipping layers). Study how the source-receiver offset, sound speed profile, noise and bottom properties influence the received signal.

Assignment given: 28. January 2008
Supervisor: Hefeng Dong, IET

Modelling of Wave Propagation in Shallow Water Environment

Skjalg Andersson

Spring 2008

Abstract

PlaneRay, an acoustic underwater propagation model based on ray tracing and plane-wave reflection coefficients, has been used to model wave propagation in shallow water environments. The program has emulated a seismic vessel towing a source-receiver setup and represented the shape of the sea floor as time responses plotted for a fixed source-receiver distance over an increasing source range. The effects of the water's sound speed profile and the sea floor's topography have been studied in detail, and the program's robustness and capability to handle these problems have been discussed and found satisfying.

Preface

This master thesis in the subject marine acoustics has been written by Skjalg Andersson spring 2008 at The Norwegian University of Science and Technology (NTNU). I want to thank my professor Hefeng Dong at the Department of Electronics and Telecommunications for her help and endless patience. I also want Svein Arne Frivik at Western Geco for the assignment and encouragement throughout the semester. Finally I would like to thank Jens M. Hovem for letting me trouble him ever so often with "stupid" questions.

Trondheim, 20.6.2008

Skjalg Andersson

Contents

List of Tables

List of Figures

1 Introduction

The effect of sound speed profiles in different shallow water configurations is to be investigated. The speed of sound is affecting the different propagation events, depending on sea floor topography and streamer depth. To predict how the combination of bathymetry and

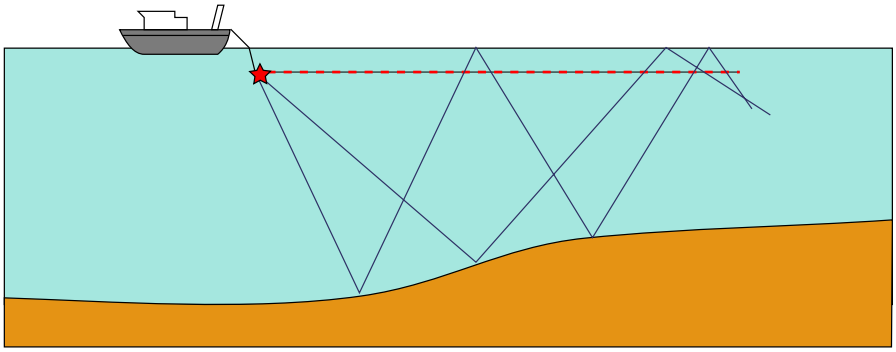

Figure 1: Shallow water wave propagation.

sound speed profile will effect the received signal, the scenarios are run through a model for underwater wave propagation. This thesis explains how this model is constructed, as well as describes its limitation and possibilities.

1.1 Background

The scenarios investigated will have the source and receiver move (being towed) over different sea floor topographies, including a dipping seafloor and a case with a sea mount in the middle of the model. The water depths will vary between 35 and 150 meters, and the source and receiver (streamer) will be placed on various depths (2.75 to 25 meter). The source and receiver distances will be from 0 to 500 meters, where each individual receiver generates synthetic seismograms. The seismograms will not contain any information of the subsurface, as only the waves moving through the water column are recorded. Finally we look at the different arrivals (direct, surface reflected and bottom reflected incl. multiples) and assess the effect of the environment on these events.

PlaneRay, a `Matlab` based program developed by Jens M. Hovem at the Norwegian University of Science and Technology has been used to carry out the wave propagation modelling. The program uses ray tracing to map the trajectories and traveltimes of a large number of eigenrays connecting the source to the receivers. The complete time response for every receiver along the streamer line are calculated, and by calculating a new time response for every new source position the synthetic seismograms are made up. The original program has been altered to be able to handle the problems presented in this paper, i.e. moving the source-receiver setup over the bottom. By looping over

the source position and running the program once for every iteration, large quantities of data is stored, allowing the user to look at a wide span of source receiver spacings. The receiver resolution when plotting the seismograms can be as small as 5 meters, which makes it possible to detect small variations in the bottom topography. It is important to point out that PlaneRay is by no means a finished product, but still has a lot of bugs and problems to solve. It is constantly under development at NTNU, and some of the problems encountered in this work might have been fixed in newer versions.

Sound speed profiles are provided by Western Geco, but in addition some known analytical expressions are used (linear increasing/decreasing speed of sound) to verify the model. The topographies are constructed.

1.2 Outline

The project is divided into 6 sections; Theory, Methods, 3 different Case sections and finally Conclusion. The first section, *Theory*, gives the reader an introduction to what physics and theories are used to describe underwater acoustics, ray tracing and how the PlaneRay program is built. *Methods* explains how the modelling is carried out in detail for the different cases and how the results are presented. The 3 *Case* sections contain the results and discussion for the different topographies and sound speed profile combinations. The conclusion and suggested future work is presented in the last section.

2 Theory

In this chapter the most relevant and important topics and theories concerning underwater acoustics are presented to give the reader some understanding of physics behind the work done in this study.

2.1 Underwater Acoustics

The field of underwater acoustics is a well developed, and the amount of background material is immense. The background theory presented here can be found in *Computational Ocean Acoustics* [4] and *Marine Acoustics* [3].

2.1.1 Sound Speed Profile

It is customary to express the sound speed in the ocean as an empirical function of three independent variables: temperature (T) in degrees centigrade, salinity (S) in parts per thousand, and depth (z) in metres,

$$c = 1449.2 + 4.6T - 0.055T^2 + 0.00029T^3 + (1.34 - 0.01T)(S - 35) + 0.016z \quad . \quad (1)$$

An illustration of a sound speed generated by equation 1, called a *sound speed profile* or *ssp* for short, is shown in figure 2. Although the sound speed is dependent of all three variables mentioned, it is considered to be dependent only of *depth* throughout this paper.

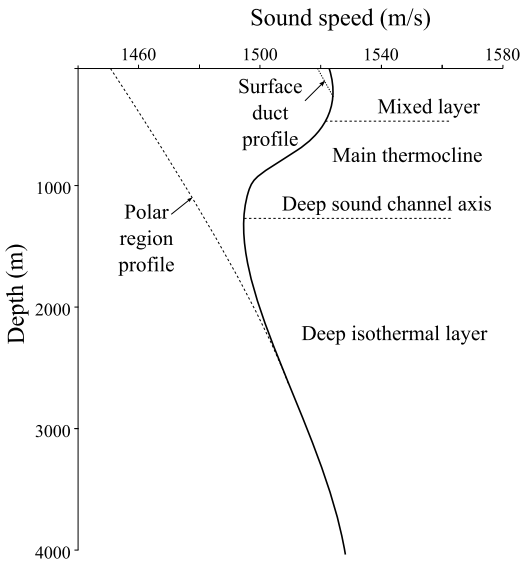

Figure 2: Generic sound-speed profiles.

2.1.2 Snell's law

Figure 3 shows how an incident wave Φ_i with angle θ_1 at the interface between two media with different sound speed (c) and density (ρ) produces a reflected wave Φ_r with the same angle and a transmitted wave Φ_t with angle θ_2.

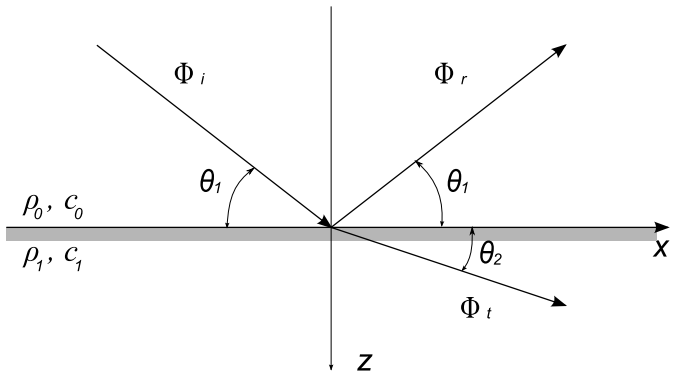

Figure 3: Reflected and transmitted wave at a interface between two media.

Incident wave

$$\Phi_i = \Phi_{i1} \exp(i\kappa_1 x \cos\theta_1 + i\kappa_1 z \sin\theta_1) \exp(-i\omega t) \tag{2}$$

Reflected wave

$$\Phi_r = \Phi_{r1} \exp(i\kappa_1 x \cos\theta_1 - i\kappa_1 z \sin\theta_1) \exp(-i\omega t) \tag{3}$$

Transmitted wave

$$\Phi_t = \Phi_{t2} \exp(i\kappa_2 x \cos\theta_2 + i\kappa_2 z \sin\theta_2) \exp(-i\omega t) \tag{4}$$

At an interface between two fluid media, the vertical particle velocity and the pressure must be the same on both sides of the interface,

$$\frac{1}{i\omega\rho_1}\frac{\partial p_1}{\partial z} = \frac{1}{i\omega\rho_2}\frac{\partial p_2}{\partial z} \tag{5}$$

and

$$p_1 = p_2, \tag{6}$$

where $p_1 = \Phi_{i1} + \Phi_{r1}$ and $p_2 = \Phi_{t2}$. For simplicity, the incident wave amplitude is often normalized, and the amplitudes of the two remaining waves are denoted R and T.

$$R = \frac{\Phi_{r1}/\Phi_{i1}}{\Phi_{i1}/\Phi_{i1}} = \frac{\rho_2 c_2 \sin\theta_1 - \rho_1 c_1 \sin\theta_2}{\rho_2 c_2 \sin\theta_1 + \rho_1 c_1 \sin\theta_2} \quad . \tag{7}$$

$$T = \frac{\Phi_{t2}/\Phi_{i1}}{\Phi_{i1}/\Phi_{i1}} = \frac{2\rho_2 c_2 \sin\theta_1}{\rho_2 c_2 \sin\theta_1 + \rho_1 c_1 \sin\theta_2} \quad . \tag{8}$$

The coefficients can be expressed with *acoustic impedance*, defined as

$$Z = \rho c \quad . \tag{9}$$

so that

$$R = \frac{Z_2 - Z_1}{Z_2 + Z_1}, \quad T = \frac{2Z_2}{Z_2 + Z_1} \quad . \tag{10}$$

From (6) it is easy to see that

$$1 + R = T \exp[i(k_2 \cos\theta_2 - k_1 \cos\theta_1)x] \tag{11}$$

Because the left side is independent of x, the right side must be independent as well. This gives us

$$\kappa_1 \cos\theta_1 = \kappa_2 \cos\theta_2 = k \quad , \tag{12}$$

where the constant k is the horizontal wave number. This is commonly know as *Snell's law*, often presented as

$$\frac{\cos\theta_1}{c_1} = \frac{\cos\theta_2}{c_2} \quad . \tag{13}$$

By dividing the water column into a finite number of layers with similar density ρ_0 and with different sound speed, Snell's law can be utilized to calculate the wave's path through the water. This is commonly know as *Ray Tracing* and is described in more detail in section 2.2

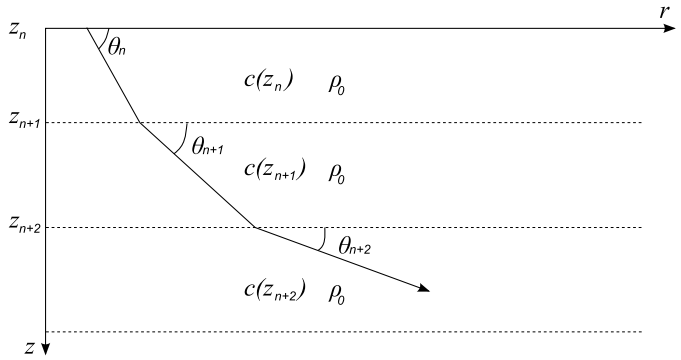

Figure 4: Snell's law applied to calculate the wave propagation through a water column with a sound speed varying with depth.

When the wave reaches the sea floor, we will at a certain distance reach a *critical gracing angle*. This angle is a limit where there is perfect reflection for all angles below, and is found from Snell's law

$$\theta_c = \arccos\left(\frac{c_1}{c_2}\right) \quad . \tag{14}$$

This critical angle only exists if the sound speed of the second medium is higher than that of the first.

2.1.3 Transmission Loss

Transmission loss is defined as the ratio in decibels between the acoustic intensity $I(r, z)$ at a field point and the intensity I_0 at 1-m distance from the source.

$$\begin{aligned} TL &= -10 \log \frac{I(r,z)}{I_0} \\ &= -20 \log \frac{p(r,z)}{p_0} \quad \text{[dB re 1m]}, \end{aligned} \tag{15}$$

where the last coupling comes from the fact that the intensity in a plane wave is proportional to the square of the pressure amplitude. Intensity is inversely proportional to the surface of the sphere, i.e. $I \propto 1/(4\pi R^2)$, where R is the distance from the source to the wavefront. Spherical spreading, near field ($r \leq z$)

$$TL = 20 \log r \quad \text{[dB re 1m]}. \tag{16}$$

Cylindrical spreading, far field ($r \gg z$)

$$TL = 10 \log r \quad \text{[dB re 1m]}. \tag{17}$$

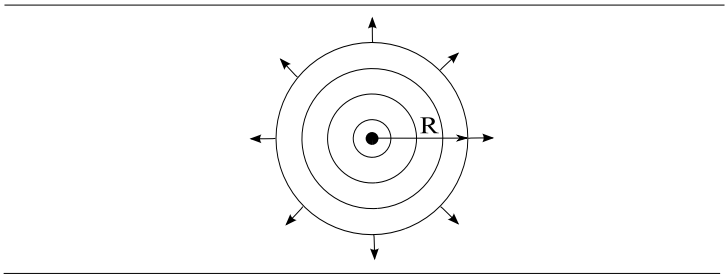

(a) Spherical spreading, near field approximation.

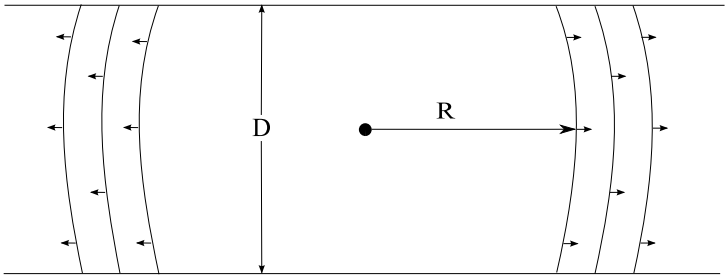

(b) Cylindrical spreading, far field approximation.

Figure 5: Geometrical spreading laws.

2.2 Ray Tracing

The theory of ray acoustics is based on the assumption that sound follows rays that are normal to surfaces with the same phase, and is described in great detail in [1]. From a point source in a medium with constant sound speed, the phase fronts form surfaces that are concentric circles and the sound will follow straight paths out from the sound source. If the sound speed is not constant, the sound rays will no longer be straight, but follow curved paths (figure 6). Ray tracing is a high-frequency approximation as it is applicable to frequencies where the wavelength is considerably smaller than the characteristic distance of the variations in the sound speed.

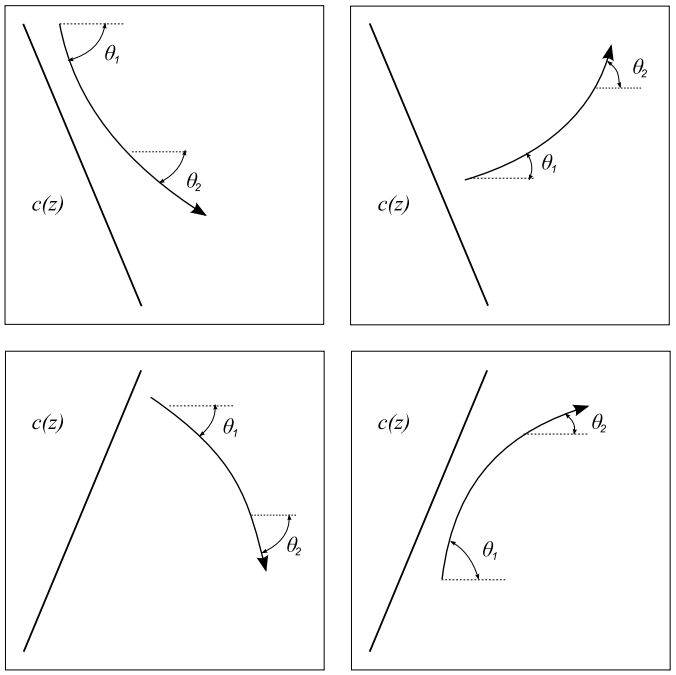

Figure 6: The four types of sound path curvatures that can occur, depending on the sound speed profile and the rays initial angle.

The sound path in a layer with a constant gradient is a circular arc with radius R (equation 18). Figure 7 on the following page shows the case with a positive gradient and the sound speed increasing with depth.

$$R = \frac{1}{|g|}\frac{c\,(z)}{\cos\theta\,(z)} = \frac{1}{\xi|g|} \quad . \tag{18}$$

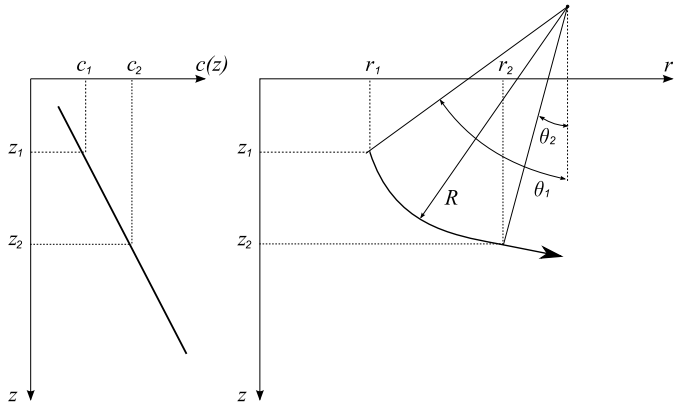

Figure 7: Ray path calculation with constant sound speed gradient.

The radius of the sound path's curvature as a function of depth z is

$$\begin{aligned} R(z) &= -\frac{c(z)}{\cos\theta(z)}\frac{dz}{dc(z)} \\ &= -\frac{c_0}{\cos\theta_0}\frac{1}{g(z)} \\ &= -\frac{1}{\xi g(z)} \quad , \end{aligned} \tag{19}$$

where ξ is known as the *ray parameter* and is defined as

$$\xi = \frac{\cos\theta_s}{c(z_s)} \quad . \tag{20}$$

θ_s is the initial angle of the ray's trajectory at the starting depth z_s where the sound speed is $c(z_s)$. The ray's range increment after traveling through a layer from the depth z_i to z_{i+1} is

$$r_{i+1} - r_i = -R_i(\sin\theta_{i+1} - \sin\theta_i) \quad , \tag{21}$$

which can also be expressed as

$$r_{i+1} - r_i = \frac{1}{\xi g_i}\left[\sqrt{1-\xi^2c^2(z_{i+1})} - \sqrt{1-\xi^2c^2(z_i)}\right] \quad . \tag{22}$$

The local sound speed gradient is approximated by

$$g_i = \frac{c(z_{i+1}) - c(z_i)}{z_{i+1} - z_i} \quad , \tag{23}$$

and the travel time increment is

$$\tau_{i+1} - \tau_i = \frac{1}{|g_i|}\ln\left(\frac{c(z_{i+1})}{c(z_i)}\frac{1+\sqrt{1-\xi^2c^2(z_i)}}{1+\sqrt{1-\xi^2c^2(z_{i+1})}}\right) \quad . \tag{24}$$

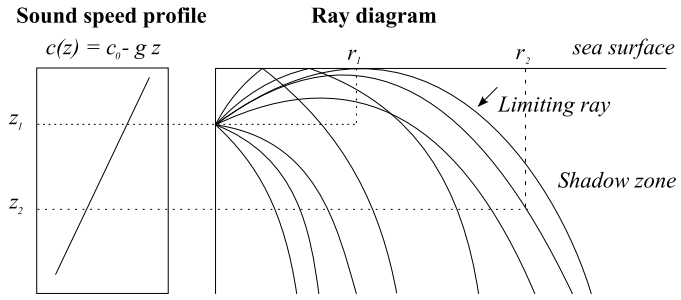

(a) Negative sound speed gradient - shadow zone.

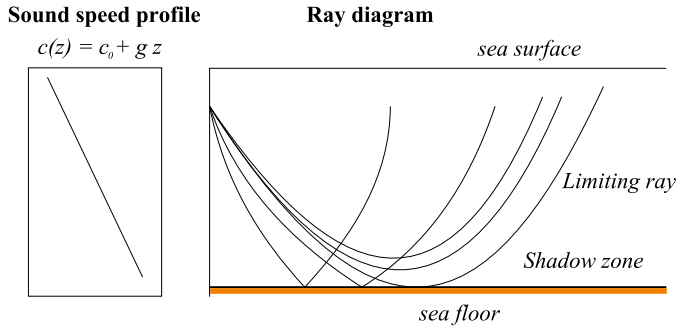

(b) Positive sound speed gradient - shadow zone.

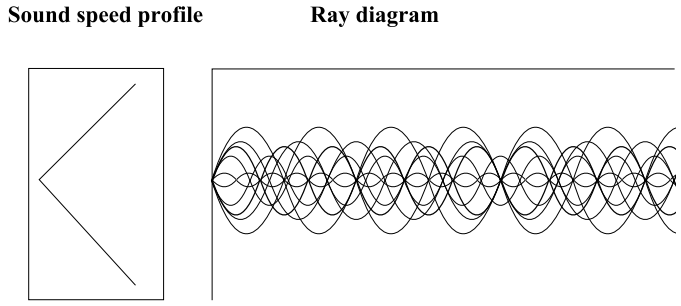

(c) Altering sound speed gradient - sound channel.

Figure 8: Altering ray trajectories as result of the sound speed gradient.

Figure 8 shows how the different sound speed gradients will effect the wave propagation. Shadow zones are defined as the part of the water that is not reached by a direct ray. All rays entering this area has either had an interaction with the sea floor or the surface. A sound channel is the special case when the sound gradient changes from negative to positive, trapping rays inside a certain angle and resulting in a large concentration of sound.

If the depth of the water column varies with range the ray parameter is no longer constant, but will change with the bottom angle. An incoming ray with angle θ_{in} will be reflected with the angle θ_{ref} when the bottom angle is α.

$$\theta_{ref} = \theta_{in} + 2\alpha \quad , \tag{25}$$

and consequently the ray parameter will change to

$$\begin{aligned} \xi_{ref} &= \frac{\cos\theta_{ref}}{c} = \frac{\cos(\theta_{in} + 2\alpha)}{c} \\ &= \xi_{in}\cos(2\alpha) - \frac{\sqrt{1 - \xi_{in}^2 c^2}}{c}\sin 2\alpha \quad . \end{aligned} \tag{26}$$

2.3 PlaneRay

PlaneRay is a ray tracing program for underwater acoustic propagation modelling of range-varying scenarios, developed by Jens M. Hovem at the Norwegian University of Science and Technology [2]. Although the program allows for range-varying scenarios, i.e. varying topography like a sloping bottom or an underwater mound, the water's sound speed can only vary with depth. The program determines a large number of eigenrays that connect a source to several receivers positioned on a horizontal line. The eigenrays are not traced into the the bottom, but modelled by local plane wave reflection coefficients. By multiplying the frequency spectrum with the spectrum of a source signal and inverse Fourier transforming the product, the complete time responses at any position along the receiving line can be synthesized. The model can be described in three stages.

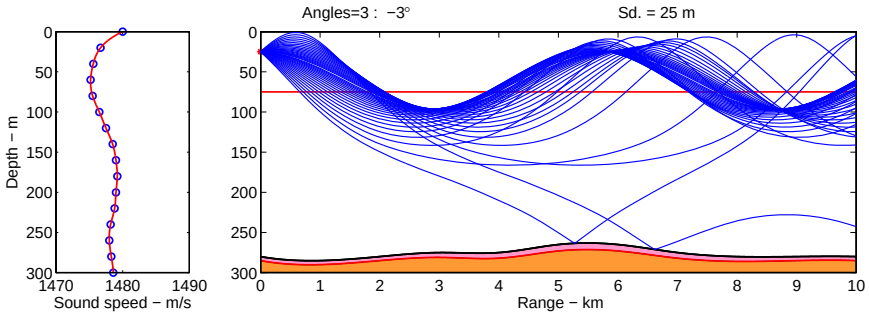

Figure 9: Example of output from the PlaneRay program with the sound speed profile (left figure) and bottom topography as input. The rays are traced throughout the the range set by the user and time responses can be calculated for every position along the receiver depth (red line).

1. The entire sound field is mapped by producing a large number of rays.
2. The trajectories of the eigenrays connecting the source to an arbitrary point on the selected receiver depth are found, and the rays are sorted with respect to their history, i.e. the number of interactions with the boundries.
3. The time response at a given receiver position is calculated by adding the contribution of every eigenray and Fourier transforming.

2.3.1 Initial Ray Tracing

To create the model environment, the program needs a sound sound speed profile and a bottom topography specified by the user, where the source and receiver line is positioned in depth and range. Figure 10 shows an example of this, where the source and receiver line

is presented as a red star and line, respectively at 2.75 and 5 meters. The ray tracing is

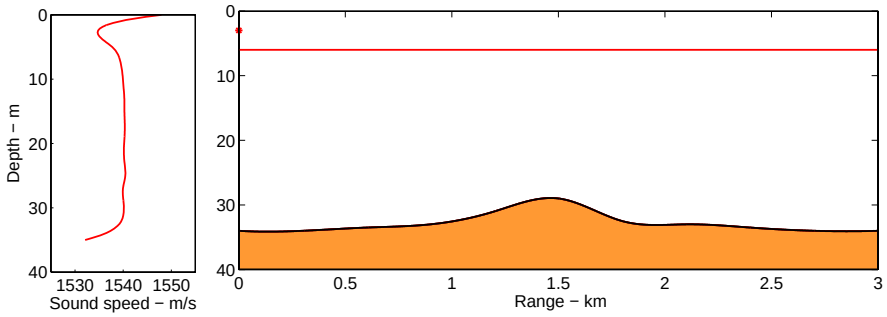

Figure 10: PlaneRay user input.

done by launching a large number of rays with angles selected to cover the space between the fixed source location and the receiver line at the specified depth. For each ray, the model computes the travel times and ranges to the locations where the ray intersects the receiver depth, and records the locations and the angles for reflection from the bottom and the surface. All this information is stored and used in the following stages. Normally you would only need to carry out this step once per site, but because the program is used to emulate a towing seismic vessel, this initial ray tracing is necessary to repeat every time there is a change in the source (boat) position. The program emulates the ocean's continuous sound speed profile by dividing the water column into a large number of equally thick layers (discretizing) where each layer has a constant sound speed, and the basic principles of ray tracing as described in section 2.2 is used to compute the ray path. That is for the layer $z_i < z < z_{i+1}$ the sound speed is

$$c(z) = c_i + (z - z_i)g_i \quad , \tag{27}$$

where c_i is the sound speed at depth z_i and g_i is the sound speed gradient. Since each layer of the water column has a constant gradient, the ray's path within a respective layer is a circular arc with a curvature radius given by equation 19 on page 8, and the rays' range and traveltime are calculated by equations 22 and 24.

2.3.2 Sorting and Interpolating

Figure 11 on the facing page shows three rays to reach three receivers at the same depth, but at different ranges from the source. All three rays have one reflection from the surface and two reflection from the sea floor, they have the same *ray history*. The rays received at ranges r_1 and r_2 are from the initial ray tracing, but the ray of interest is positioned somewhere between them at point r_0 with an initial source angle θ_0. Since all rays have the same number of interactions from the boundaries, the relation between θ_0 and receiver range is expected to follow a smooth curve suitable for interpolation. The example shown in this figure is generalized and implemented in the program as shown in table 1 on the next page, in this case corresponding to *Class 5* with n = 2.

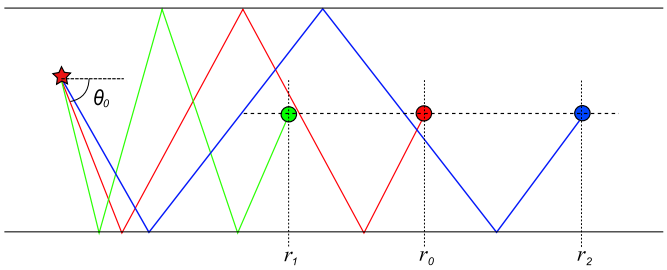

Figure 11: An eigenray to the receiver at range r_0. is found by interpolating between the two rays arriving at the same receiver depth at ranges r_1 and r_2.

Table 1: Rays sorted in classes with similar ray histories. The first 5 classes are applicable when you have the special case of a constant sound speed profile, while the rest is discretized by whether the ray has an upper or lower turning point.

Class	**Bottom**	**Surface**	
Class 1	0	0	Direct wave
Class 2	n-1	n	Pos and neg start angle
Class 3	n	n	Positive start angle
Class 4	n	n	Negative start angle
Class 5	n	n-1	Pos and neg start angle
Class	**Bottom**	**Upper turning points**	
Class 6	n	n+1	Negative start angle
Class 7	n	n	Positive start angle
Class 8	n	n	Negative start angle
Class 9	n+1	n	Positive start angle
Class	**Surface**	**Lower turning points**	
Class 10	n+1	n	Positive start angle
Class 11	n	n	Positive start angle
Class 12	n	n	Negative start angle
Class 13	n	n+1	Negative start angle
Class	**Upper turning points**	**Lower turning points**	
Class 14	n+1	n	Negative start angle
Class 15	n	n	Positive start angle
Class 16	n	n	Negative start angle
Class 17	n	n+1	Positive start angle

2.3.3 Synthesis of the sound field

The sound field is synthesized by coherent additions of the contributions of every eigenray (figure 12). PlaneRay uses the ray history shown in table 1 to divide the eigenrays into either *direct-*, *refracted-* and *upper/lower turning* rays. These ray classes are stored and plotted separately, which eliminates the problem of noise from the source. Because of some instabilities in the PlaneRay program Transmission loss from the interactions with the sea floor is calculated.

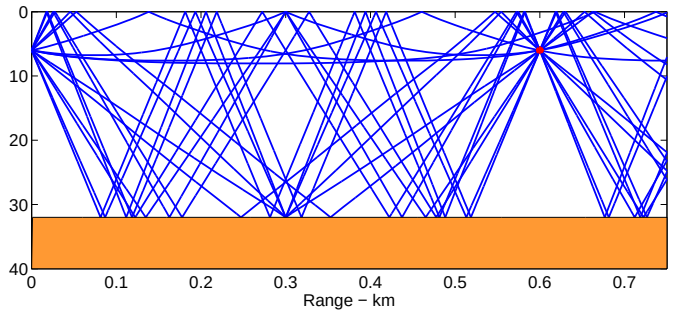

Figure 12: Example of several eigenrays connecting a source to a receiver along the receiver line.

The addition of the eigenrays for different source-receiver distances are presented as time responses, an example shown in figure 13. The y-axis of the plot is the length of the receiver line, in this case 1 km, and the x-axis is the traveltime from the source to the receiver.

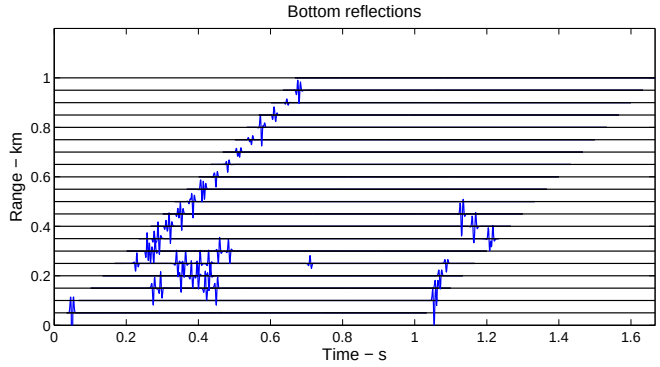

Figure 13: Example of time responses recorded for receivers spaced 50 meters apart up to a range of 1000 meters.

A short Ricker pulse is used as source signal throughout the entire thesis, and the time- and frequency response of the signal is shown in figure 14.

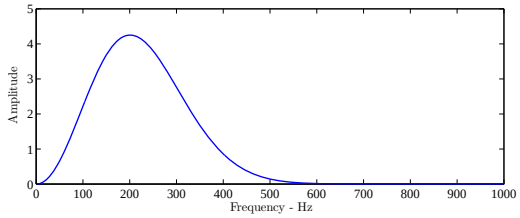

(a) Frequency response.

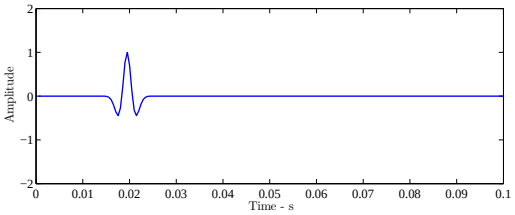

(b) Time response.

Figure 14: The source signal and its frequency spectrum used in the calculations of the time responses.

3 Methods

3.1 Sound speed profiles

The following sound speed profiles are a selection from the sound speed profiles made available by Western Geco (see appendix A). They were all recorded off the coast of Africa, but differ in what date and time of day they are recorded. The profiles in the selection where chosen because they vary in depth and velocity and have distinct properties that will allow us to study sound speed channels, shadow zones etc.

Sound Speed Profile 1: The sound speed profile shown in figure 15 is extracted from the data `TOPSEQ004eol`. The transition from a negative to a positive sound speed gradient in the top 5 meters of the profile should result in a sound channel with an axis at the minimum were sound will be concentrated, dependent on the depth of the source. The rather constant sound speed from 5 to 30 meters should result in a straight ray without any curvature, while the strong negative gradient at the bottom will result in a downward curvature. To investigate the influence of the sound channel the source and receiver depth is varied while the bottom topography remain unchanged.

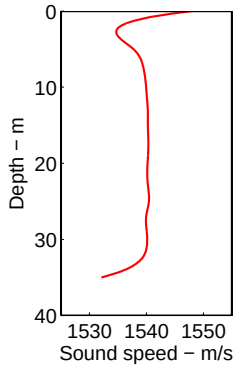

Figure 15: Sound speed profile from file TOPSEQ004eol.txt

Sound Speed Profile 2: Figure 16 extracted from `TOPSEQ004mar_01` show a profile with a slight negative gradient. The maximum depth of this sound speed profile is a lot deeper than the other profile investigated. Because of the negative gradient in the upper part of the profile we will get a shadow zone at a certain distance from the source, dependent of the source depth, where we will not receive any direct waves.

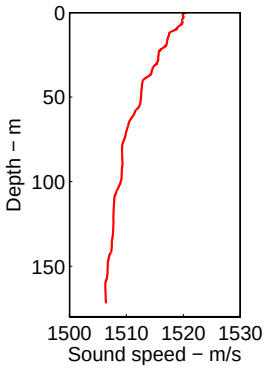

Figure 16: Sound speed profile from file TOPSEQ004mar_01.txt

Sound Speed Profile 3: The sound speed profile shown in figure 17 is generated to have a simple and known sound speed profile to compare with the other profiles and to help verify the results from the program.

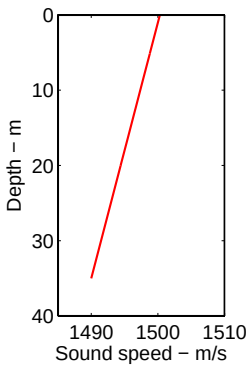

Figure 17: Sound speed profile from file TOPSEQ004nsea_04.txt

3.2 PlaneRay Setup

The initial setup of the PlaneRay program requires the user to set environmental parameters and input files. The parameters that describe the environment is depth, range, bottom shape, bottom properties and the input sound speed profile of the water column. The bottom properties are fixed to a random value since this study doesn't cover bottom interactions and transmission loss. Additional parameters for the ray tracing has

Table 2: Environmental parameters.

Depth	0 - 150 [m]
Range	0 - 3.000 [m]
Topography	Varying
Cp_0	From files
ρ_0	1000 $[kg/m^3]$
Cp_1	1700 [m/s]
Cs_1	0 [m/s]
ρ_1	1500 $[kg/m^3]$

to be chosen as well, e.g source and receiver depth, source position increment, receiver resolution, range, number of rays and angle resolution, and ray interactions with the boundaries. These parameters can be set different by the user from case to case, but for simplicity most of them have been fixed throughout this study. The original program has been altered to be able to handle the cases investigated. The setup is required only once per case, and the program will then loop over the source position. The increase in source range is fixed to 10 meters for all cases investigated. The receiver spacing for each source loop is 5 meters. The flow of the program is described in section 2.3, and the data and figures are stored sequentially. To simulate a receiver line being towed behind a boat, time responses as shown in figure 21 are calculated for different source

Table 3: Ray tracing parameters.

Source depth	2.75-25 [m]
Receiver depth	2.75-25 [m]
Source increment	10 [m]
Receiver resolution	5 [m]
Receiver range	0 - 3.000 [m]
Number of rays	2000
Angle resolution	38 [deg]
Maximum interactions	4

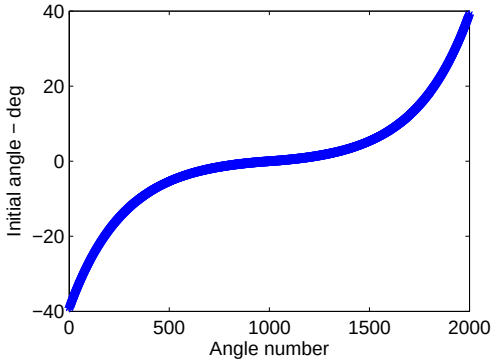

Figure 18: The angle resolution used throughout the study.

positions. In all cases investigated in this thesis, the source is moved 10 meters before another time response is calculated (figure 19)- giving us a total of 100 time responses for every 1000 meters covered. Each of these 100 time responses contain data from receivers spaced 5 meters apart along the receiver line. With the receiver line ranging from 1000 to 3000 meters, the amount of recordings are between 20.000 and 60.000 for every case.

The recorded data is stored with information on the source position and the source-receiver distance, which gives us the opportunity to plot the time responses for a given source-receiver distance as a function of source position, as shown in figure 22. This plot gives a representation of the sea floor, which is the goal of the ray tracing. Different source-receiver spacings and sound speed profiles are compared to investigate on what effects they will have on the recorded signal.

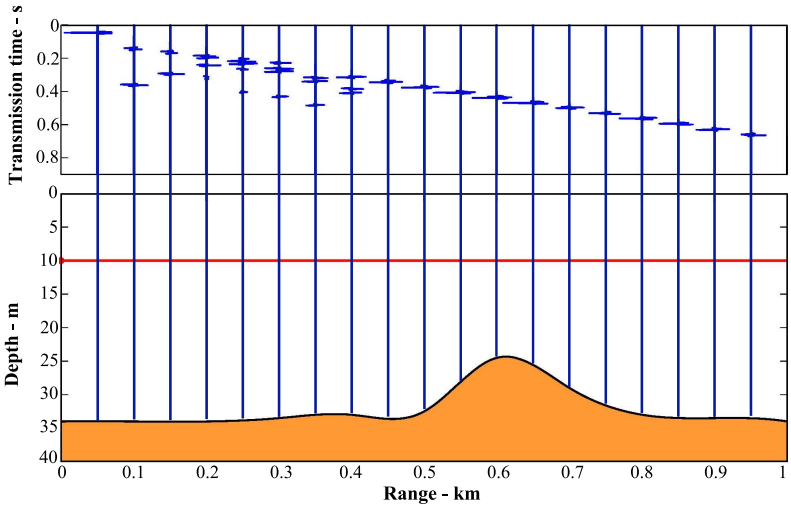

Figure 19: Example of the signals recorded by receivers equally spaced along a receiver line at 10 meters depth. In this case there are 50 meters between two neighboring receivers, yielding 20 recordings along a 1000 meters line.

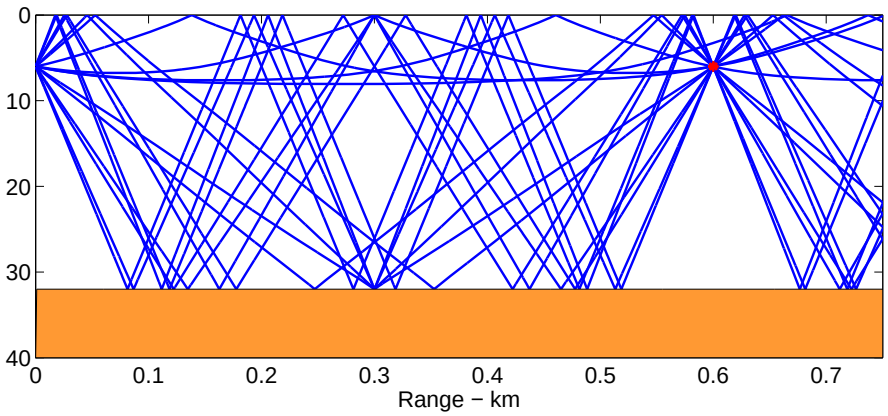

Figure 20: The signal recorded at a given receiver position is calculated by adding the eigenrays intersecting the receiver location.

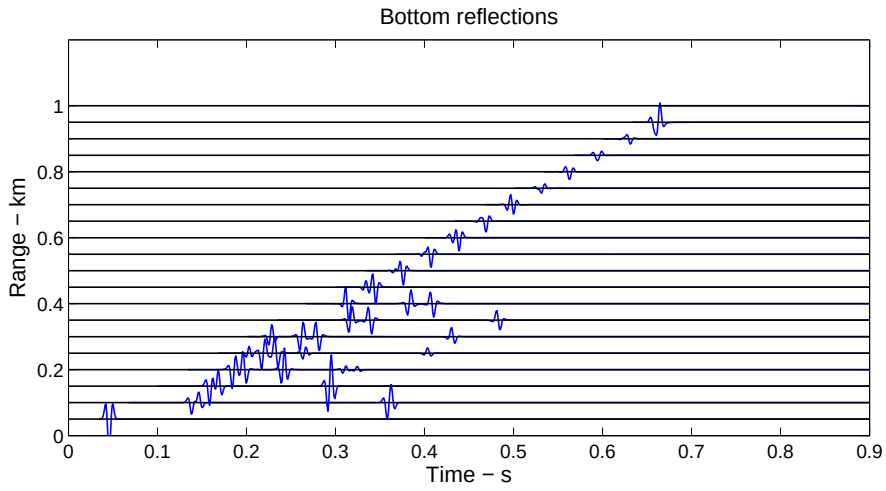

Figure 21: The top part of figure 19 with shifted axes. The time delay from the source to the receiver along the x-axis, and source-receiver distance along the y-axis.

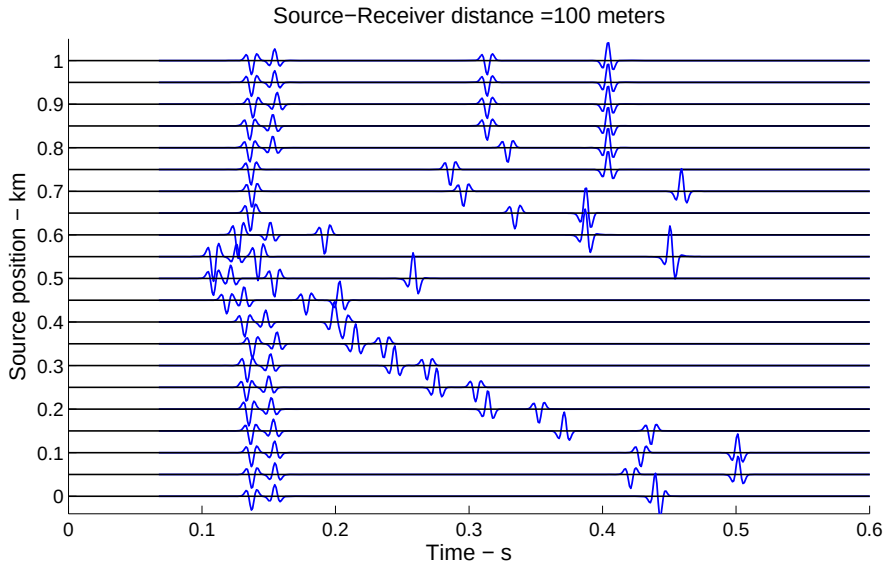

Figure 22: Time responses for a given source-receiver distance, in this case 100 meters, as a function of source position along bottom and arrival time of the recorded signal.

3.3 Programming

Some modifications of the original PlaneRay model was necessary to implement the moving source. Early attempts to implement this had the source range increase over a fixed sea floor. This caused convolution errors in the computation of the time responses. This was omitted by rather moving the sea floor towards a fixed source position. A total of 18 cases were tested, and all the case data and source files are supplied with the disc attached at the back of this paper. The cases are

```
------ CASES ---
CASE 1: SSP1 - 2.75 meters - Large mound
CASE 2: SSP1 - 6 meters - Large mound
CASE 3: SSP1 - 10 meters - Large mound
CASE 4: SSP1 - 2.75 meters, 1500 range
CASE 5: SSP1 - 2.75 meters, 1500 range - small mound
CASE 6: SSP1 - 6 meters, 1500 range - small mound
CASE 7: SSP1 - 10 meters, 1500 range - small mound
CASE 8: SSP2 - Sloping Bottom - 10 meters
CASE 9: SSP2 - Small mound 6 meter
CASE 10: SSP2 - Small mound 10 meter
CASE 11: SSP2 - Small mound 25 meter
CASE 12: TEST SSP - Large mound 2.75 meter
CASE 13: SSP2 - Sloping Bottom - 25 meters
CASE 14: SSP3 - Mound - 6 meters
CASE 15: TEST SSP - Large mound, 20 spacing
CASE 16: SSP1 - Slope - 2.75 meters
CASE 17: SSP1 - Slope - 6 meters
CASE 18: SSP2 - Slope - 10 meters
```

The step by step execution of the PlaneRay program, and how to rerun the cases (or run new ones) are given in appendix B.

4 Topography - Mound

The first case we will investigate is wave propagation over an underwater mound (see figure 23). The mound is roughly 300 meters wide and the height will be varied as shown (purple vs. yellow). The reason why there is no values on the depth axis is because the different sound speed profiles have different maximum depth, hence the size of the mound is varied accordingly. Of interest is the received signal from shot points before, directly over and after the source/receiver has passed the mound. The source and receiver will have the same depth.

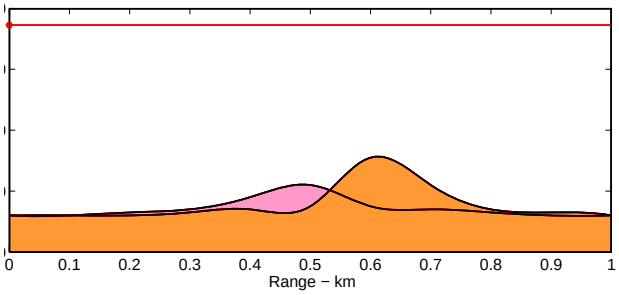

Figure 23: The topography of the two mounds that are investigated.

4.1 Sound Speed Profile 1

Table 4 shows the different ray tracing parameters used for the first sound speed profile. The different depths are chosen so that we can investigate how the sound channel will influence the rays' trajectories. Figure 24 (a) shows the first run of the program for the

Table 4: SSP 1 - Ray tracing parameters.

Source depth	2.75, 6 and 10 [m]
Receiver depth	2.75, 6 and 10 [m]
Source increment	10 [m]
Receiver resolution	5 [m]
Receiver range	0 - 1.000 [m]
Number of rays	2000
Angle resolution	38 [deg]
Maximum interactions	4

biggest mound, which for this specific sound speed profile is approximately 10 meters in height. The source- and receiver depth are 2.75 meters, which is the depth of the sound channel axis. For illustrative purposes the rays that reach the bottom are stopped, and the effect of the sound channel is evident. Only higher angle rays will escape the channel

and reach the bottom, giving us poor illumination of the sea floor with increasing distance from the source. Figures 24 (b) and (c) show how the effects of the sound channel are reduced by placing the source and receivers deeper than the sound channel axis. The number of rays are the same for all three cases. Figure 25 (a) show the eigenrays recorded

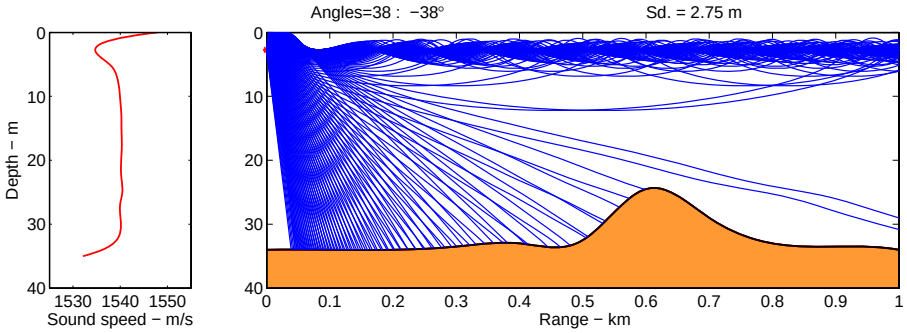

(a) Source and receiver depth 2.75 meters.

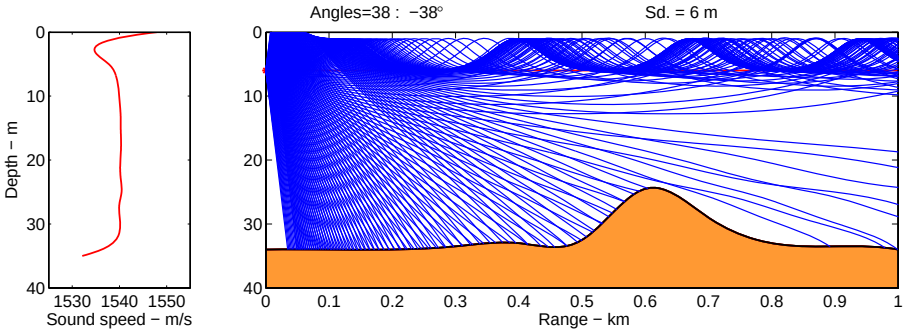

(b) Source and receiver depth 6 meters.

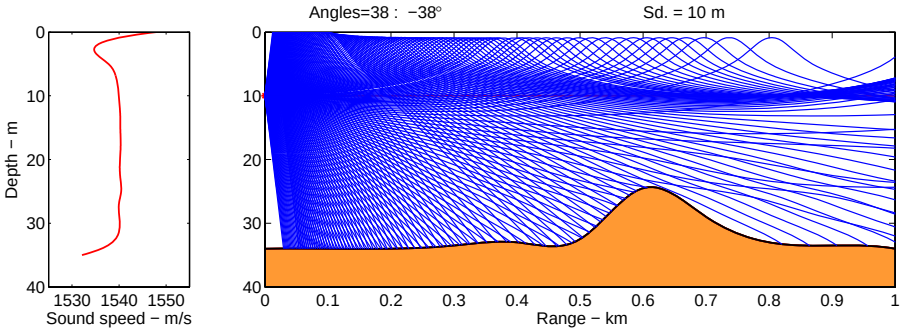

(c) Source and receiver depth 10 meters.

Figure 24: Influence of source depth.

at 500 meters when the source and receiver is positioned at the sound channel axis. When the source and receiver is moved down to 10 meters (b), more rays illuminate the seafloor and bring information back to the receiver. (c) shows how the surface reflected wave will reach the receiver when the source-receiver distance is short enough.

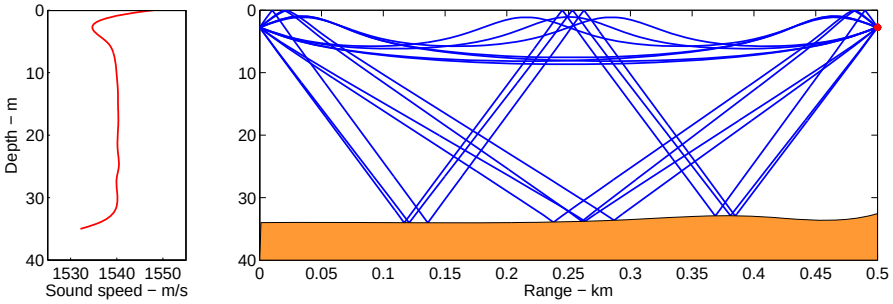

(a) Recorded eigenrays at 500 meters at sound channel axis depth.

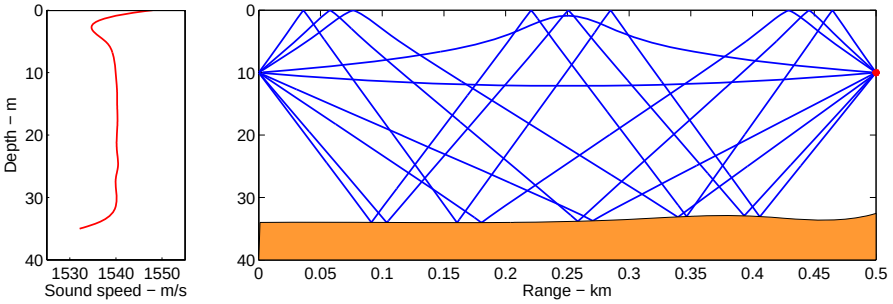

(b) Recorded eigenrays at 500 meters at 10 meters depth.

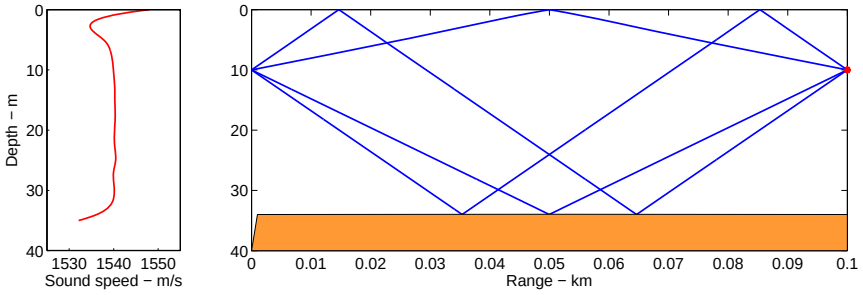

(c) Recorded eigenrays at 100 meters at 10 meters depth.

Figure 25: SSP1 eigenrays

4.1.1 Results

The plots in figure 26 show the time responses for source-receiver distances varying from 100 to 400 meters, with a source depth of 2.75 meters. In the top 2 plots the shape of the mound is evident, and different wave arrivals can be distinguished. Particularly the first plot with source-receiver spacing only 100 meters contain some very late arrivals. These

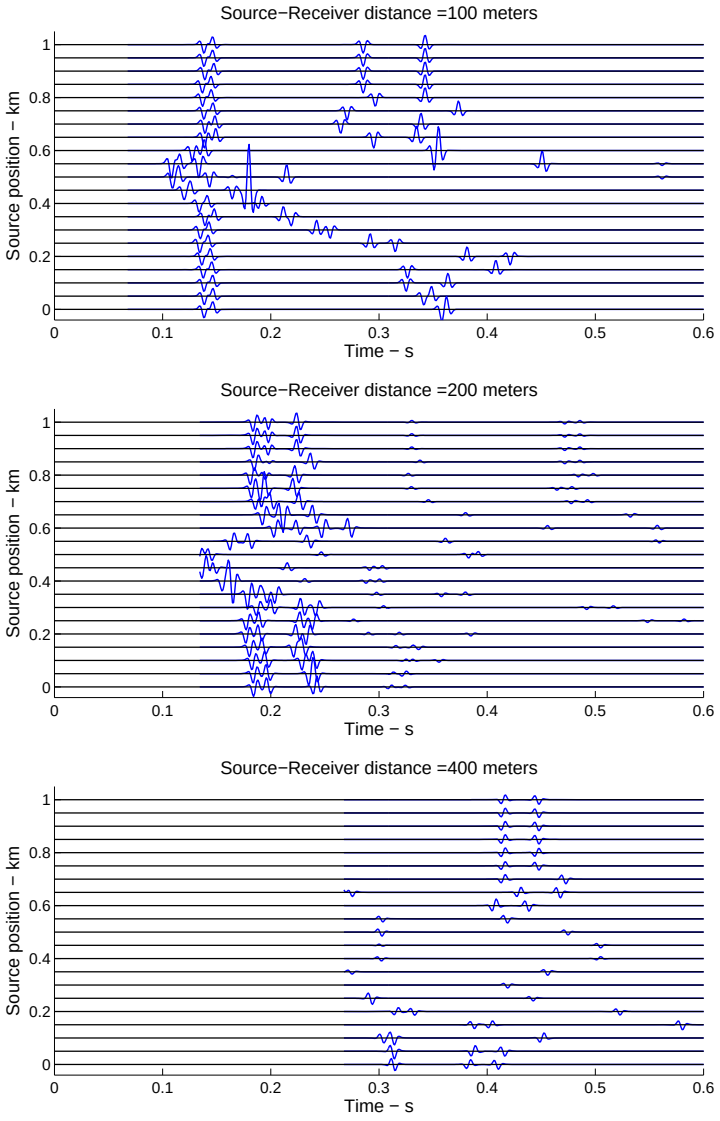

Figure 26: Recorded time responses at 2.75 meters with varying source-receiver spacing.

waves are the ones that has interacted with the surface and the sea floor 2 times, and thus have traveled a longer distance. The bottom plot shows the received signal at 400 meters source-receiver spacing, and it is impossible to recognize the shape of the mound.

There are too few rays intersecting with the receiver at this location, and the more you increase the source-receiver distance, the worse the received signal gets (figures are not included in the paper).

The plots in figure 27 show the time responses for source-receiver distances varying from 100 to 400 meters, with a source depth of 6 meters. Apart from some changes in the time axis it is almost identical to the 2.75 meters source depth.

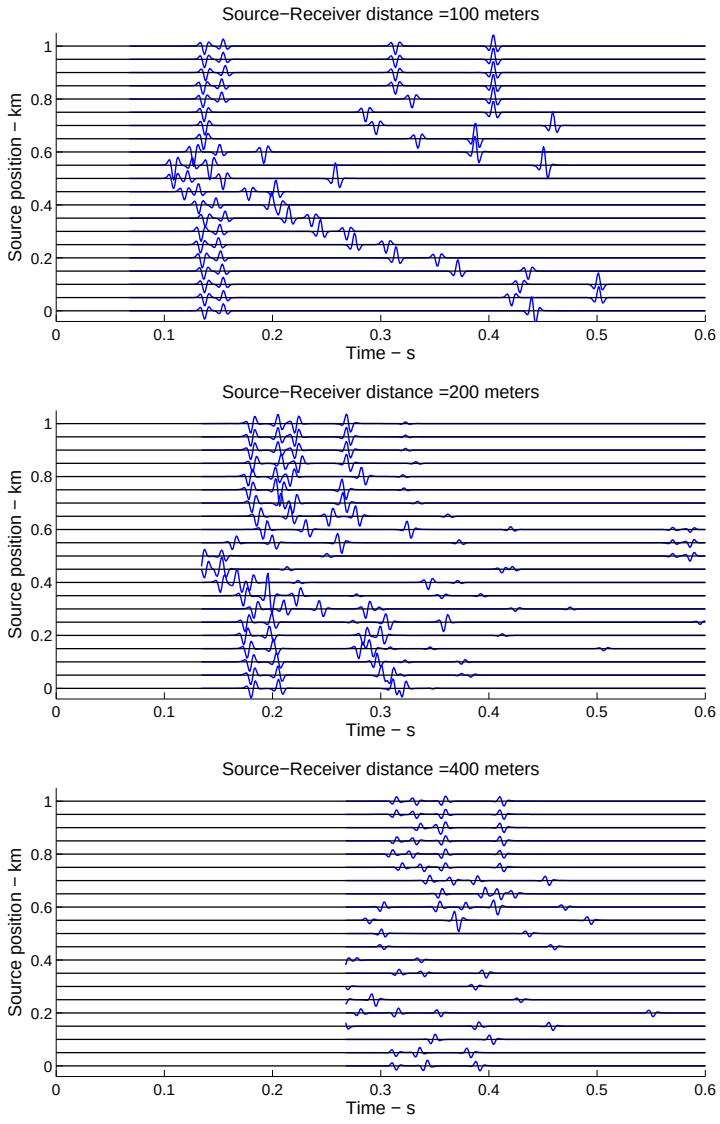

Figure 27: Recorded time responses at 6 meters with varying source-receiver spacing.

The plots in figure 28 show the time responses for source-receiver distances varying from 100 to 400 meters, with a source depth of 10 meters. The top figure shows a line of pulses arriving at approximately 0.08 seconds for all source positions. This line is the surface reflected wave shown in figure 25 on page 25 (c). These surface reflected waves are also evident in figure 30 on page 30 (a) for all source-receiver depths.

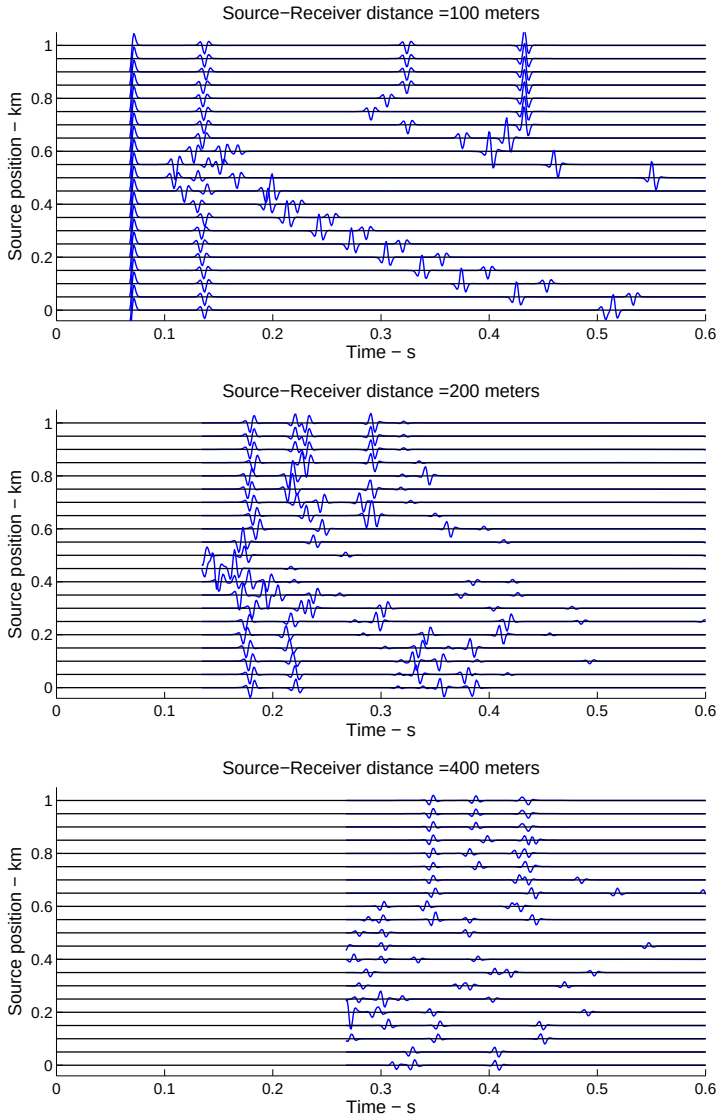

Figure 28: Recorded time responses at 10 meters with varying source-receiver spacing.

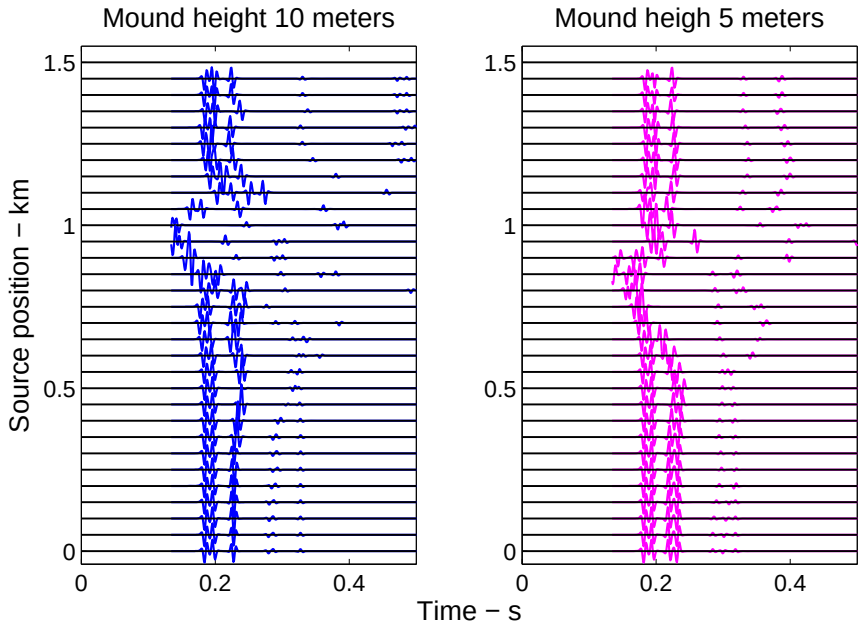

Figure 29: Time responses from a source depth of 2.75 meters from survey over a big mound (left - blue) and a small mound (right - purple). Source-receiver spacing is 200 meters.

Figure 29 show the comparison between the big and the small mound from figure 23 on page 23 recorded from a depth of 2.75 meters and a source-receiver spacing of 200 meters. Both the shapes and the location of the mounds match the actual topography satisfactorily.

Figure 30 on the following page shows a comparison between the received signal of a small mound for all three depths investigated for the first sound speed profile. The surface wave repeats itself in all plots as the first arrival. It is evident that for a short source-receiver distance, i.e. 100 meters, there is no striking difference between the different source-receiver depths. When the source-receiver distance is increased to 200 meters, the 2.75 source depth becomes considerably weaker than the other two, and it is more difficult to identify the shape of the mound. Both the 6 and 10 meters source depth gives a good representation of the topography. Although more difficult, it is still possible to distinguish the mound for a source-receiver distance of up to 400 meters for all three source depths.

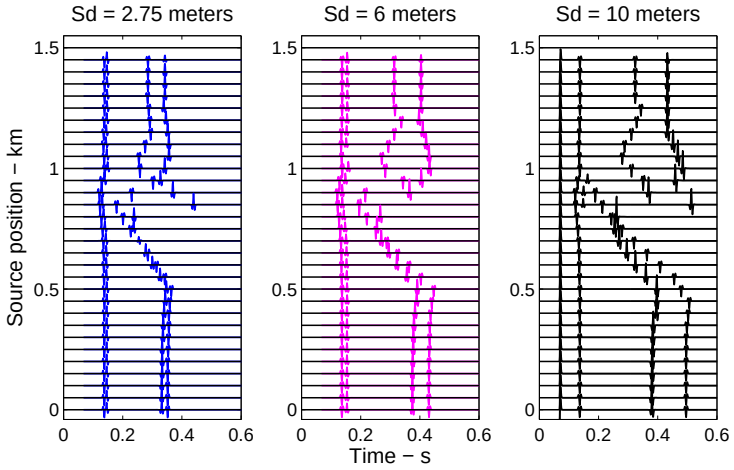

(a) Source-Receiver spacing = 100 meters.

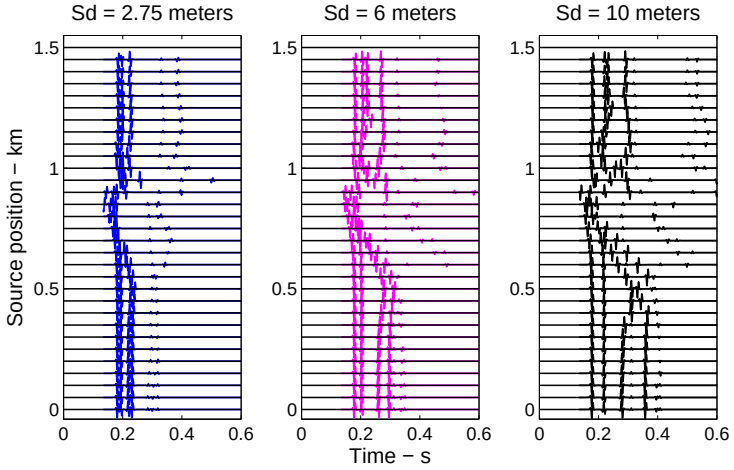

(b) Source-Receiver spacing = 200 meters.

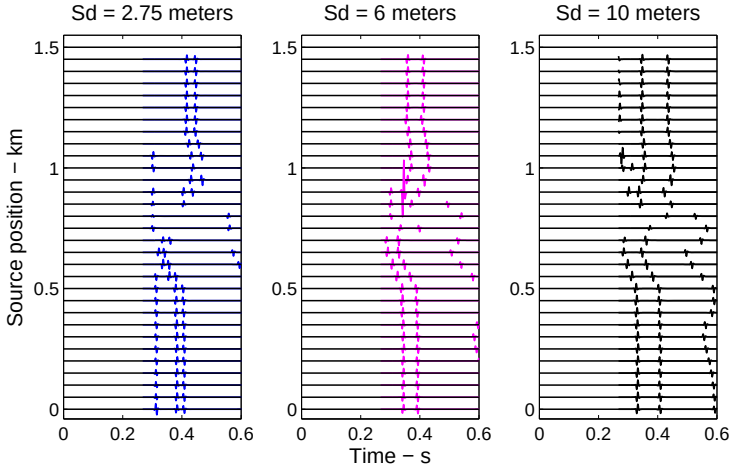

(c) Source-Receiver spacing = 400 meters.

Figure 30: Comparison of the time responses over a small mound with different source depths.

4.2 Sound speed profile 2

The second sound speed profile is with its negative gradient will bend the rays downwards and produce a shadow zone none of the direct waves will reach. This is shown in figure 31 where the shadow zone starts at approximately 950 meters. Table 5 contains the parameters for the ray tracing. The parameters are mainly the same as the previous run, but the source and receiver depths are changed and the range is increased because the sound profile is much deeper than the previous one. It is not of interest to look at that many source-receiver depths in this case, since there is no sound channel that will have any influence on where the source should be located.

Table 5: SSP 2 - Ray tracing parameters.

Source depth	6 and 10 [m]
Receiver depth	6 and 10 [m]
Source increment	10 [m]
Receiver resolution	5 [m]
Receiver range	0 - 1.000 [m]
Number of rays	2000
Angle resolution	38 [deg]
Maximum interactions	4

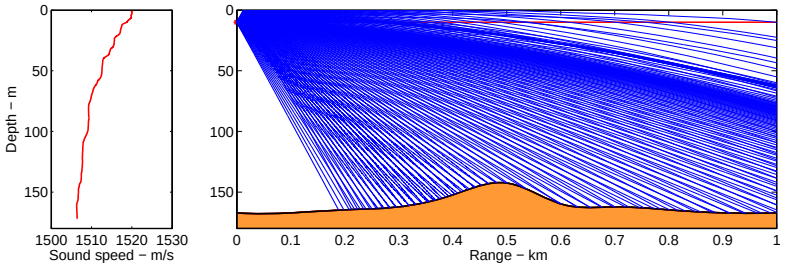

Figure 31: SSP2 over a small mound.

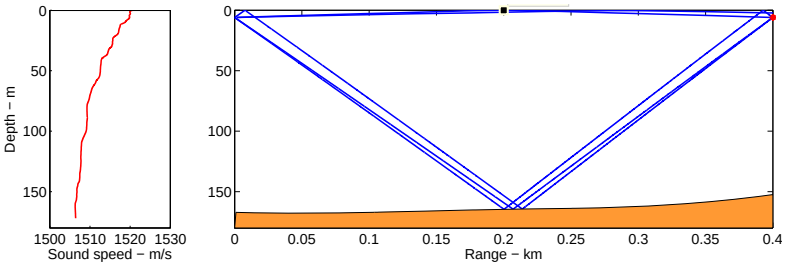

Figure 32: Recorded eigenrays at 400 meters at 6 meters depth.

4.2.1 Results

Figure 32 is included to explain the first time response in figure 33. The plot shows the recorded time response at 400 meter source-receiver spacing and contains a pulse arriving at 0.3 seconds. For presentation purposes these plots do not contain any horizontal lines. Because the receiver resolution is so high, i.e. 10 meters between each new source position, the figure would have been unreadable if the lines were there. Because of the increase in depth from the previous case, the range of the topography has been increased from 1000 to 1500 meters. As figure 33 (b) shows, the shape of the mound is clear even at

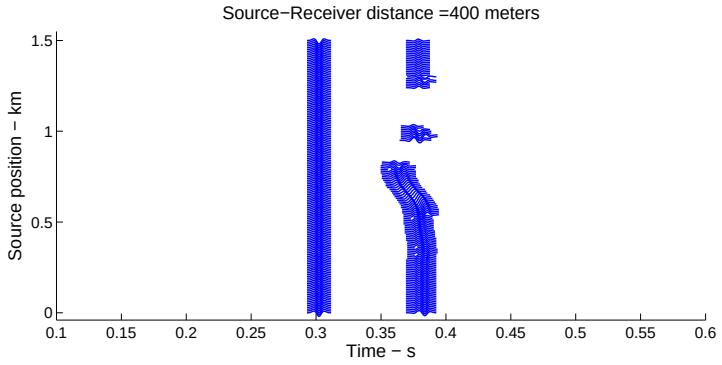

(a) Source-Receiver spacing = 400 meters.

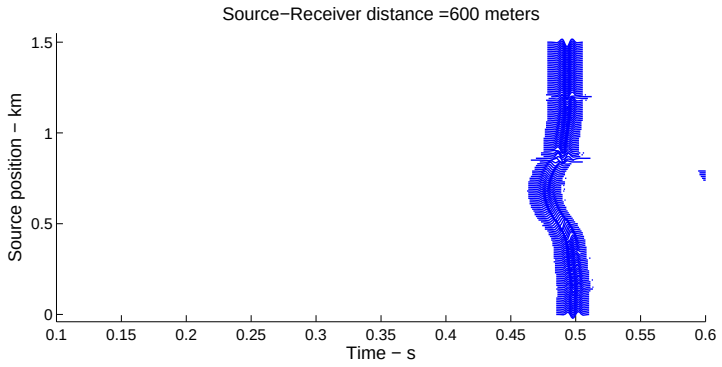

(b) Source-Receiver spacing = 600 meters.

Figure 33: Recorded time responses over a small mound at 6 meters with varying source-receiver spacing.

600 meters. At longer ranges the shape of the mound is harder to identify because the difference in travel time of the different rays becomes smaller and smaller.

4.3 Sound speed profile 3

The third sound speed profile is a constant negative gradient resulting in a shadow zone at around 300 meters. What differs this case from the two previous cases is that the angle resolution has been decreased from 38 to 18, i.e. more than halved. The result of this decrease is that there are very few rays illuminating the bottom at short source-receiver distances, as is illustrated in figure 35.

Table 6: SSP 3 - Ray tracing parameters.

Source depth	2.75 [m]
Receiver depth	2.75 [m]
Source increment	10 [m]
Receiver resolution	5 [m]
Receiver range	0 - 1.000 [m]
Number of rays	2000
Angle resolution	18 [deg]
Maximum interactions	4

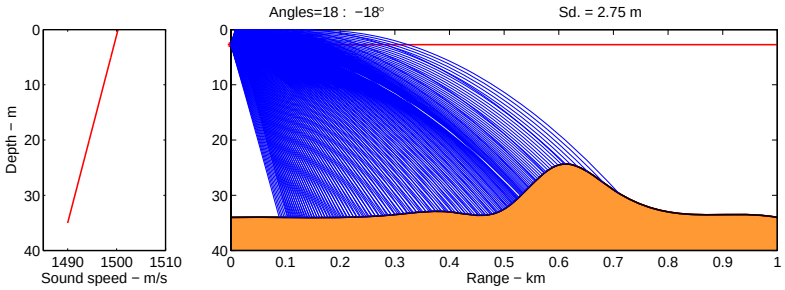

Figure 34: SSP3 over a big mound.

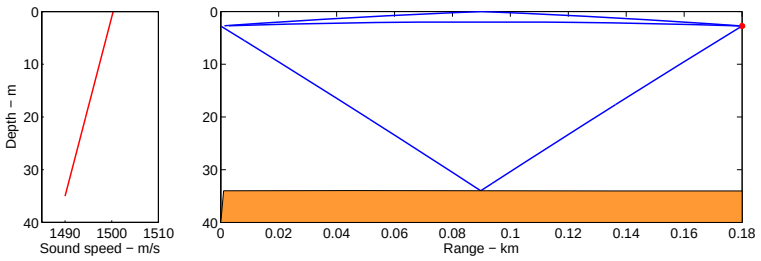

Figure 35: Recorded eigenrays at 180 meters at 2.75 meters depth.

4.3.1 Results

Figure 36 shows the only results worth presenting from this run, which only shows how important it is to choose a high angle resolution (in this case only 18 deg). The three time responses is dominated by the first arrival which is the surface reflected waves, and for the two bottom plots were the source-receiver distances are both below 200 meters the top of the mound is hardly able to detect. For some reason there are hardly any bottom reflections, even though figure 35 on the preceding page shows that a bottom reflection should be excepted for the last source-receiver spacing. Figure 37 shows the

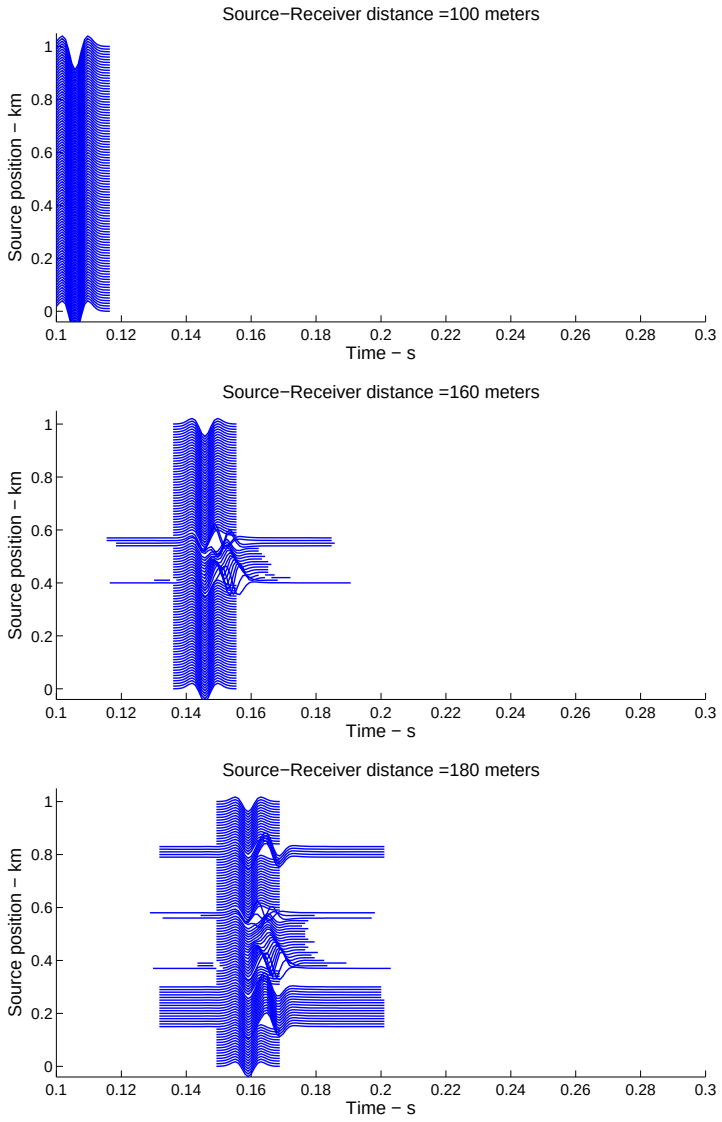

Figure 36: Recorded time responses at 2.75 meters with varying source-receiver spacing.

result of increasing the angle resolution to 38 deg. To decrease the computation time, the resolution was decreased to 20 meters, and the source-receiver spacing took steps of 100 meters pr iteration. The shape of the mound is visible on the first plot, but second one is too messy to interpret. Somehow, the surface reflected wave is not present in these plots.

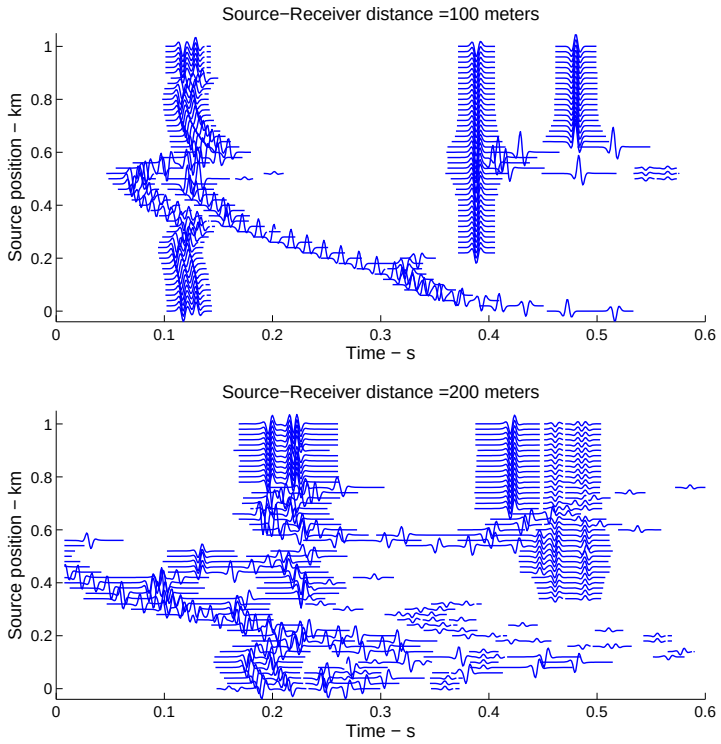

Figure 37: New recorded time responses at 2.75 meters with varying source-receiver spacing.

4.4 Discussion

The use of the PlaneRay program to model wave propagation over an altering topography, i.e. mounds of different height and length, has been shown in this section. The results are satisfactory in the sense that it is quite possible to distinguish the shape of the sea floor by plotting the time responses as function of source position with constant source-receiver spacing. For the first sound speed profile, with a sound channel in the upper part of the sound speed profile, the plots presented in figure 30 on page 30 sum up the program's abilities. The shape of the bottom is easy to distinguish for all three source-receiver depths, although the possible source-receiver distance is somewhat disappointing. Even though it is possible to observe the mound's shape for source-receiver distances of 400 meters, it is important to keep in mind that all plots presented here

have absolutely no noise present, apart from the surface reflections. If the plots would contain background noise and large numbers of direct rays because of the sound channel, it would be much harder to distinguish the shape of the mound from the noise. As long as the received bottom reflections are strong and continuous, as in e.g figure 30 (b), the noise could easily be able to filtered out. In figure 30 (c) on the other hand, the received signals are weak and the sea floor's shape is very hard to detect, limiting the useful source-receiver distance.

The second case, with a deep negative sound speed profile, caused some problems. Even though the results were good (figure 33 on page 32) the computation time was very long. The computer used was a laptop with a 1.73 GHz processor and 2.00 GB of RAM, and for this specific case it took 18 hours to run the program, and the stored data exceeded 600 Mb. The advantages of the excessive storage of data is that it allows for a high receiver resolution and many choices of source-receiver spacing. For this case the range was 1500 meters, source increment was 10 meters and the receiver spacing was 5 meters along a 1000 meters receiver line, yielding $(1500/10) \times (1000/5) = 30.000$ recordings, each containing 1024 values. This means the time responses can be plotted for every 10 meters in source position and with a source-receiver spacing varying from 5 to 1000 meters. If this is necessary or not can be discussed, but if the user doesn't know which range or receiver spacing is of interest, it is a big advantage to be able to examine the problem over a large span of positions.

The third case gave a good illustration of why it could be beneficial to set the receiver resolution and source-receiver spacing before the execution of the program. The initial run shown in figure 36 on page 34 was not adequate because the angle resolution was too small to receive any meaningful data, and it required a rerun where the angle resolution was increased. The initial run took 18 hours to compute, but by choosing before execution which source-receiver spacing and resolution we wanted to look at (in this case the source-receiver spacing was increments of 100 and the resolution was 20 meters), the computation time was shortened to only 30 minutes. Although highly time saving, the results seem to be imperfect (see figure 37 on the preceding page). The most obvious fault is the lack of surface reflected wave, but also some second arrivals without any obvious origin can be observed at 0.4 seconds.

5 Topography - Sloping bottom

The second case we will investigate is how the wave will propagate when the bottom becomes more and more shallow. The parameters for the different sound speed profiles are exactly the same as for the previous case, hence they will not be repeated here.

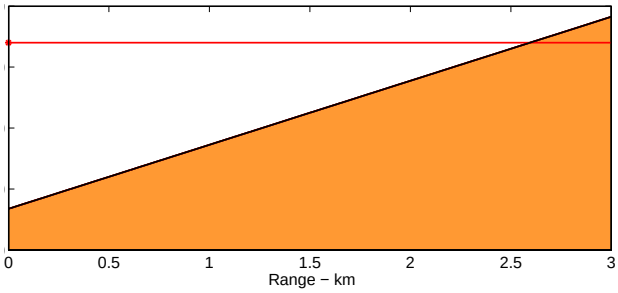

Figure 38: Sloping bottom topography.

5.1 Sound speed profile 1

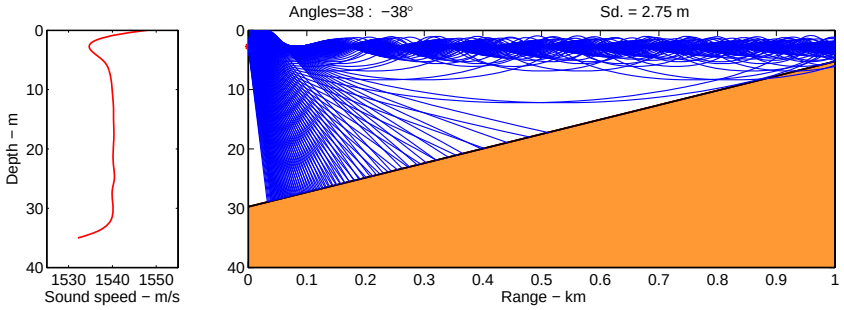

(a) Source and receiver depth 2.75 meters

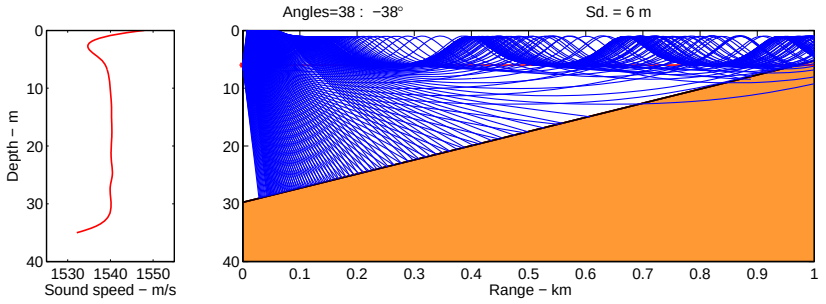

(b) Source and receiver depth 6 meters

Figure 39: Influence of source depth.

For the sloping bottom, source and receiver depth of 2.75 and 6 meters are investigated for the first sound speed profile (figure 39. In this case some errors in the program is evident, as some rays can be observed moving straight through the sea floor. Serious as it might be, the large amount of rays that are being produced still produces a good coverage and minimizes the effect of these "leaking" rays.

5.1.1 Results

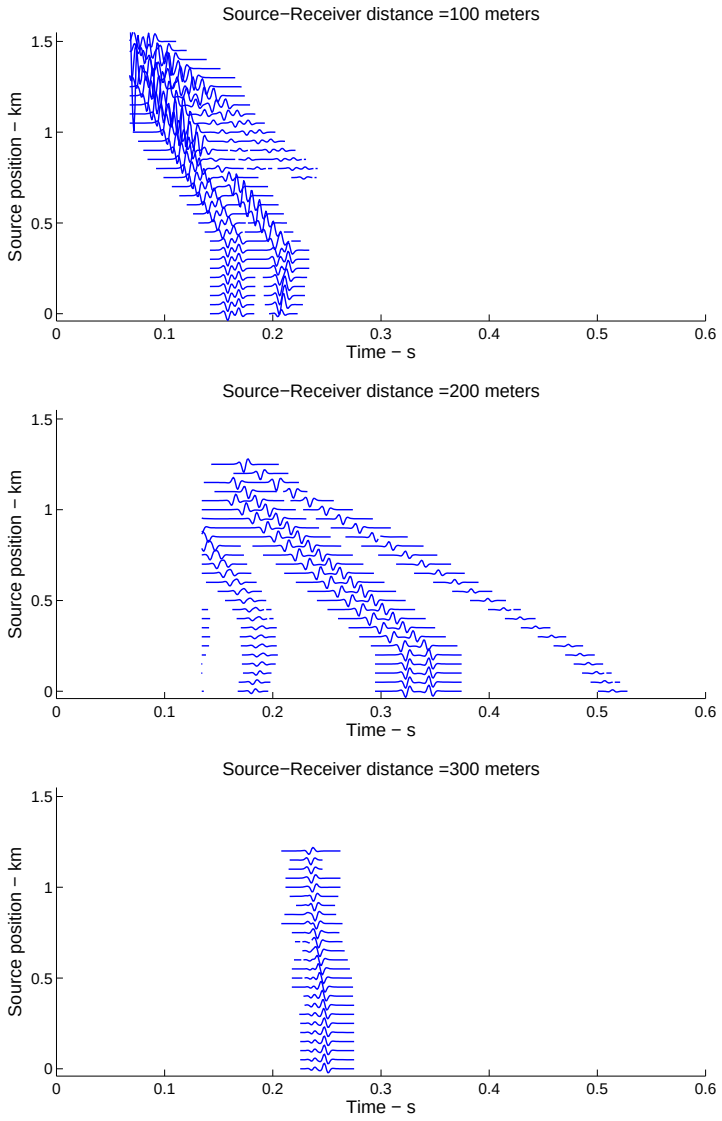

Figure 40: Recorded time responses at 2.75 meters with varying source-receiver spacing.

Figure 40 shows the recorded time responses for the 2.75 meters source-receiver depth.

The two upper plots both contain several arrivals and the slope is easily recognized. Similar to the "Mound" case, the received signal is best when the source-receiver spacing is about 200 meters. Observe that there are no surface reflections present in these plots, as can be expected from studying figure 39 on page 37 (a) and the effect of the sound channel in the upper layer of the water column. Figure 41 shows the recorded time

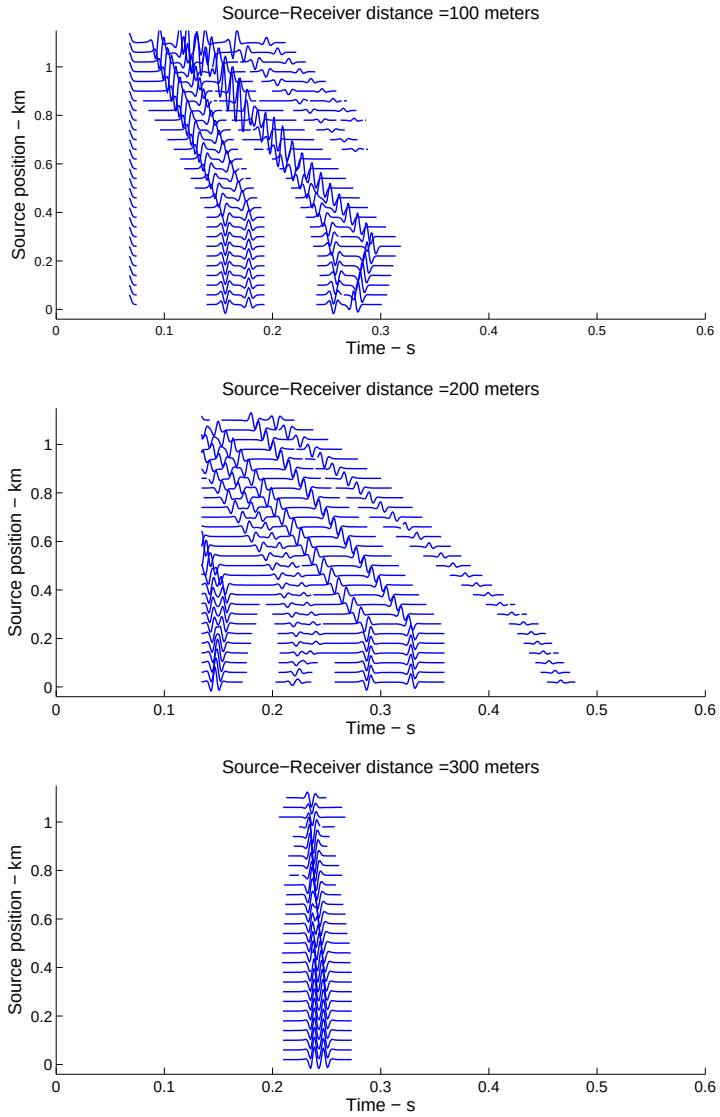

Figure 41: Recorded time responses at 6 meters with varying source-receiver spacing.

responses for the 6 meters source-receiver depth. They are practically identical to the responses for the 2.75 source depth, if you take the difference in travel time into account, except for the presence of a surface reflection for the source-receiver spacing of 100 meters.

5.2 Sound speed profile 2

The second sound speed profile is investigated for source-receiver depths of 6 and 25 meters (figure 42). In both cases the range is 1000 meters.

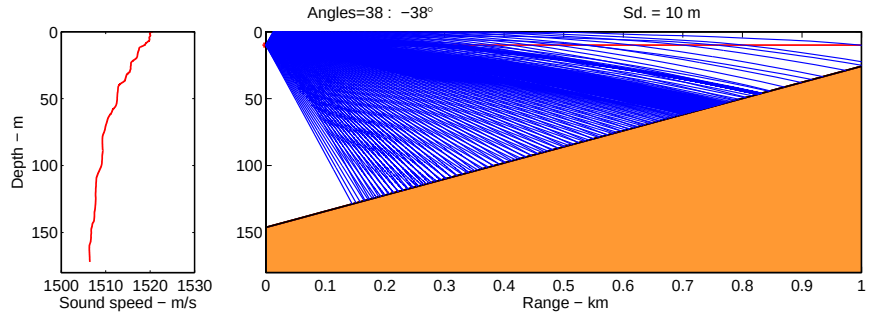

(a) Source and receiver depth 6 meters

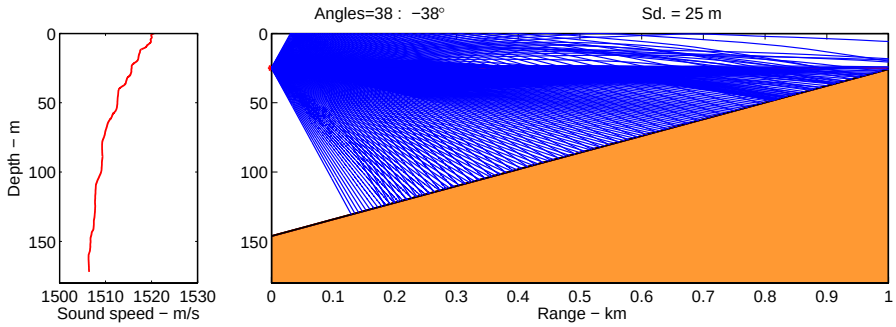

(b) Source and receiver depth 25 meters

Figure 42: Influence of source depth.

5.2.1 Results

Figures 43 and 44 show the time responses for the second sound speed profile plotted for source depths of 10 and 25 meters, respectively. The 10 meters source depth shows a nice transition in how the difference in pulse arrival times decrease with increasing source-receiver range, until they all almost arrive at the same point in time (43 - bottom). For the 25 meters source depth, the results are quite disturbing. It is impossible to recognize a sloping bottom for 100 meters source-receiver spacing, but it becomes more obvious when the spacing is increased to 200 and 500 meters.

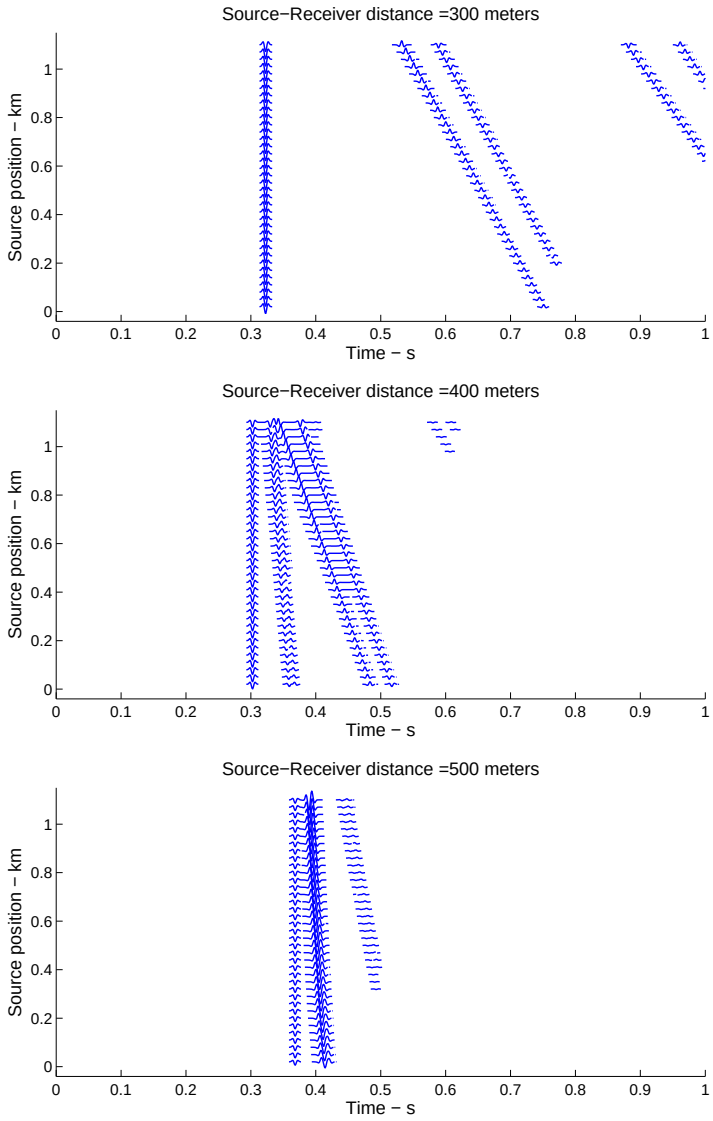

Figure 43: Recorded time responses at 10 meters with varying source-receiver spacing.

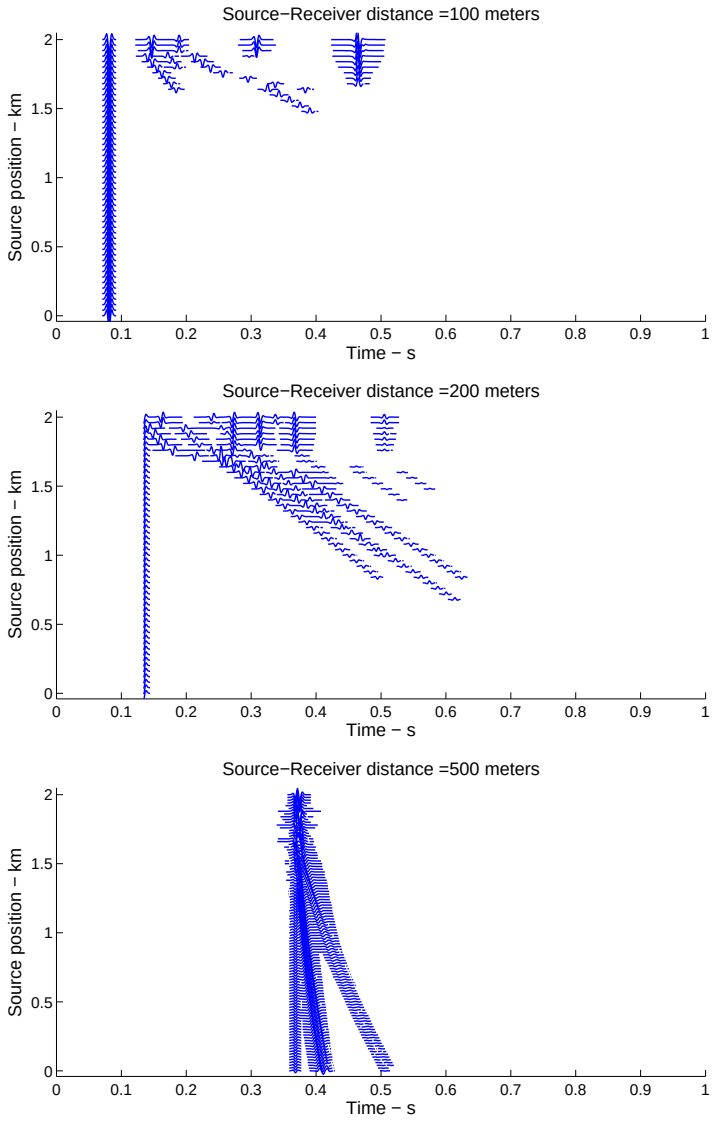

Figure 44: Recorded time responses at 25 meters with varying source-receiver spacing.

5.3 Discussion

Modelling of wave propagation across a sloping bottom has been investigated in this section. For the shallow water, i.e. the first sound speed profile with water depth of 30 to 8 meters along a 1000 meters range, the time responses give a fairly good representation of the sloping bottom (figures 40 and 41 on page 39). The deeper sound speed profile has a higher degree of differences between the source depths. Figures 43 and 44 on the preceding page show how the source depth of 10 meters produces excellent time response plots for given source-receiver distances, while the source depth of 25 meters doesn't. There is no evident reason for the bad representation of the topography in this special case, as you could expect that the deeper located receiver line would result in better representations at small source-receiver distances than the higher placed. It is obvious that some thoughts must be spent on the choice of source depth and topography range, and the user can benefit from running the case of interest for many different source depths.

6 Conclusion

In this paper we have investigated how the use of PlaneRay, an acoustic underwater propagation model based on ray tracing and plane-wave reflection coefficients, can help us model wave propagation in shallow water environments. The model, which is a `Matlab` based program has proved capable of reproducing the topography and shape of the sea floor by recording synthetic seismograms at different receiver positions and plot these as function of source position. The program's original code was developed to look at the propagation of sound from a fixed source position over large distances with varying topography and how the properties of the sea floor would influence the transmission loss of the signal. By editing the source code so that it loops over the source position, and hence moving it along the topography, and running the program for every new location, we managed to emulate a seismic vessel towing a source and receiver setup. Much of the work put into this study was the modification of the code, and how to implement the source position loop. The final version of the program, which performed satisfactorily, moved the sea floor towards the source, in contrast to moving the source along the sea floor.

The results presented in sections 4 and 5 shows how the rays' trajectories are influenced by various sound speed profiles in the water column, the water depth and the topography. We have seen how a sound channel and negative sound speed gradient influences the received signals, and which source-receiver distances are best suited. In the cases that involved a shallow water depth, i.e. less than 50 meters, a source-receiver distance between 100 and 400 meters proved the best choice. When the water depth increased, so did the optimal source-receiver distance. For a water depth of 150 meters the signals received at 400-600 meters from the source proved to best reproduce the topography.

Unfortunately we were not able to look at a noisy environment. The PlaneRay model computed both the direct waves from the source to the receivers, together with waves that would have a upper or lower turning point. When we tried to plot these signals together with the refracted signals from the surface and the sea floor, they contained no data. Since PlaneRay is still under development, we will not linger with these problems. Another problem on the other hand, that could easily be omitted, is the large amount of data stored for each source location iteration. By setting the desired source-receiver spacing and resolution before you run the program, computation time could be reduced significantly. One run where the source-receiver spacing was set to increments of 100 meters instead of every 5 meters, and the source position increment was 20 instead of 10, the computation time was reduced from 18 hours to 30 minutes. This comes at a cost as you are not able to increase resolution or look at other source-receiver distances on a later stage.

References

[1] Jens M. Hovem. Marine acoustics, the physics of sound in underwater environments. Handouts, July 2005.

[2] Jens M. Hovem. Planeray: An acoustic underwater propagation model based on ray tracing and plane wave reflection coefficients. 2008.

[3] Jens M. Hovem and Rune M. Holt. Acoustical classification of the sea-floor. Technical Report STF44 A82128, SINTEF, 1981.

[4] Finn B. Jensen, William A. Kuperman, Michal B. Porter, and Henrik Schimdt. *Computational Ocean Acoustics*, pages 1–202. American Institue of Physics, 1994.

A Sound Speed Profiles

The sound speed profiles shown underneath were supplied by WesternGeco. The name of the file of which each sound speed profile was extracted is shown on the right side of the plots.

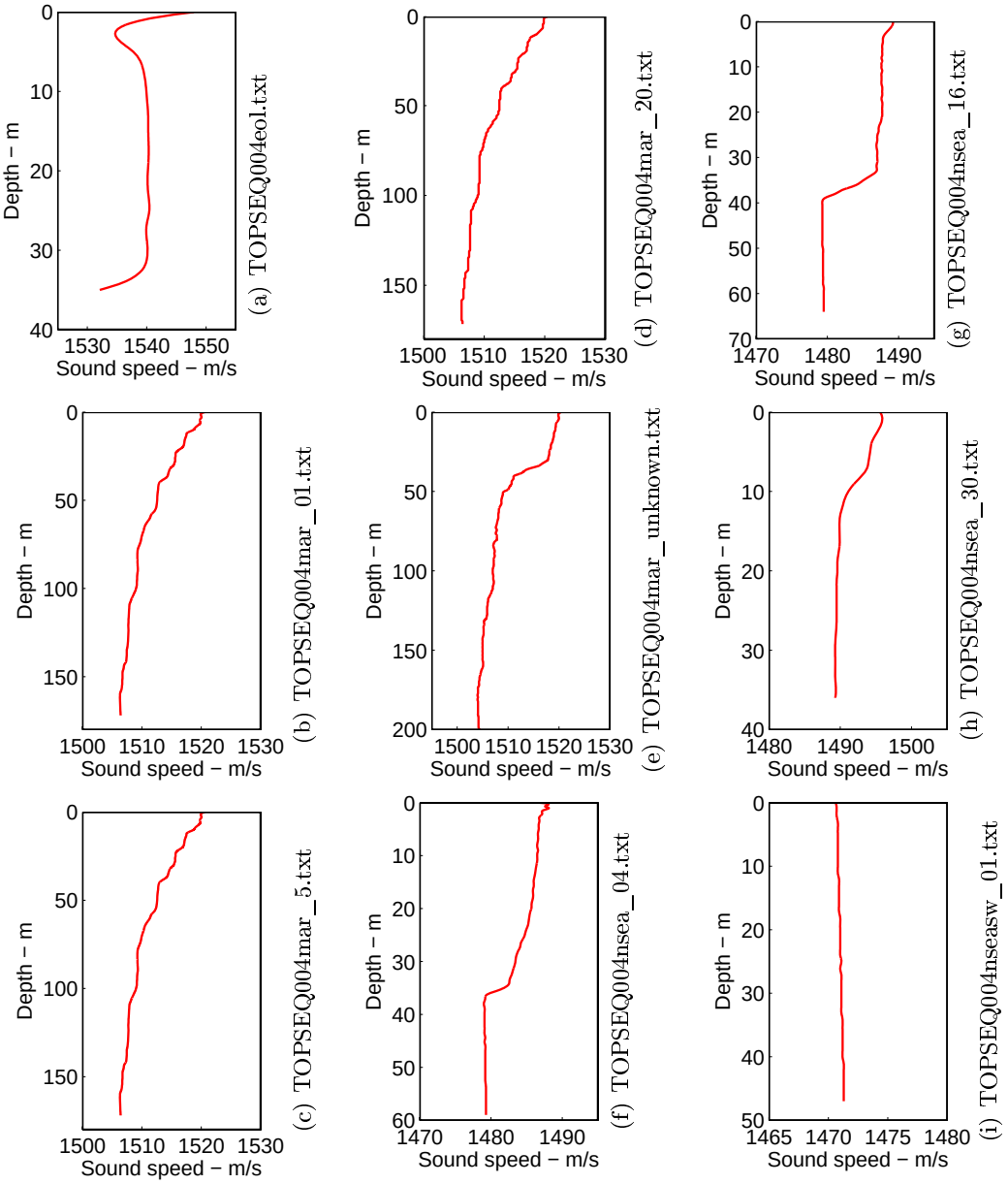

Figure 45: Investigated profiles

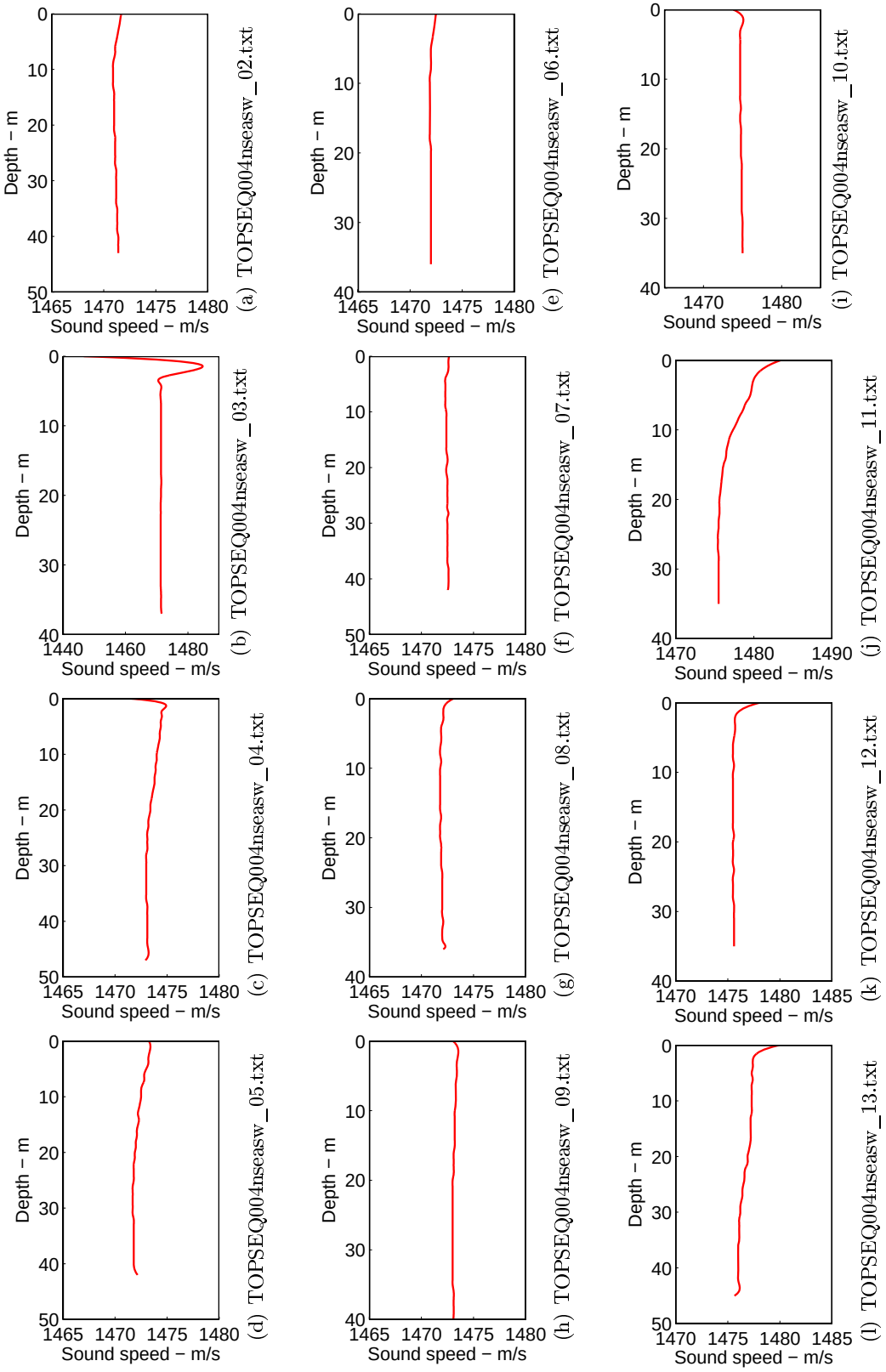
Depth – m
Sound speed – m/s
(a) TOPSEQ004nseasw_02.txt
(b) TOPSEQ004nseasw_03.txt
(c) TOPSEQ004nseasw_04.txt
(d) TOPSEQ004nseasw_05.txt
(e) TOPSEQ004nseasw_06.txt
(f) TOPSEQ004nseasw_07.txt
(g) TOPSEQ004nseasw_08.txt
(h) TOPSEQ004nseasw_09.txt
(i) TOPSEQ004nseasw_10.txt
(j) TOPSEQ004nseasw_11.txt
(k) TOPSEQ004nseasw_12.txt
(l) TOPSEQ004nseasw_13.txt

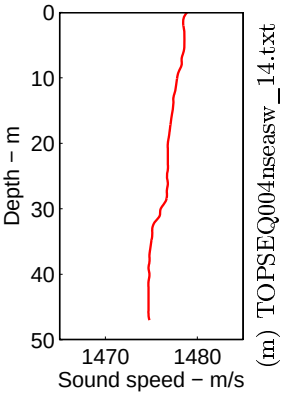

(m) TOPSEQ004nseasw_14.txt

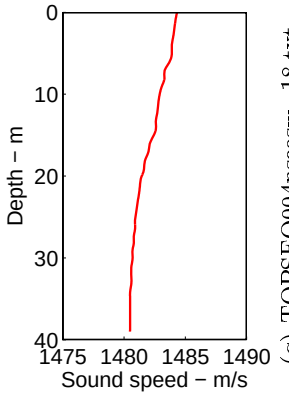

(q) TOPSEQ004nseasw_18.txt

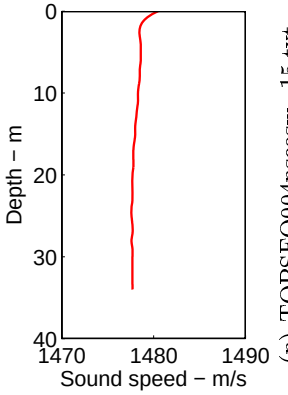

(n) TOPSEQ004nseasw_15.txt

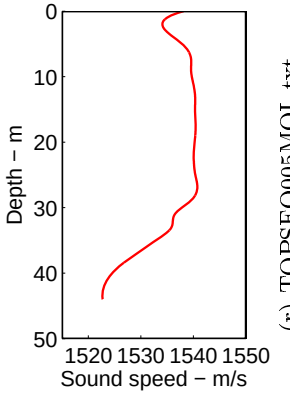

(r) TOPSEQ005MOL.txt

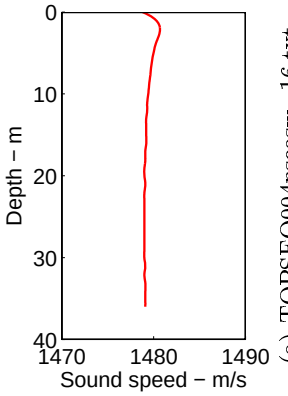

(o) TOPSEQ004nseasw_16.txt

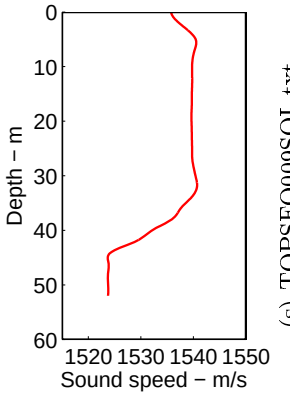

(s) TOPSEQ009SOL.txt

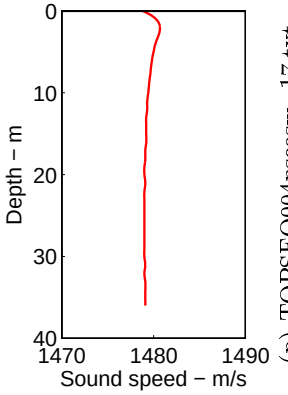

(p) TOPSEQ004nseasw_17.txt

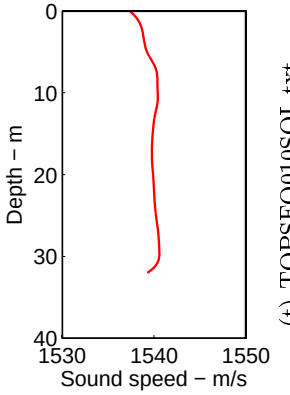

(t) TOPSEQ010SOL.txt

B PlaneRay Execution

The user inputs for the modified PlaneRay program required to produce the data and plots presented in this report are explained in this section.

1. `Loop_Plane_ray_1.m`

   `Loop_Plane_ray_1.m` is the master file. All it does is `eval` the other files and create the environment and loop over the source position. When you choose to loop over the source position the values in the `evaled` files are fixed.

```
source_increment = input('Choose source increment: ');

for 0:1:(range/source_increment)
        eval('Plane_ray_input');
        eval('Plane_ray_2');
        eval('Plane_ray_3');
end
```

2. `Plane_ray_input.m`

   `Plane_ray_input.m` is the file where you set the environmental- and some of the ray tracing parameters.

```
choice = input('Choose SSP data file: ');

bottom_stop = input('Trace rays after they...
                hit the bottom? y=0, n=1: ');

R_max = input('Choose range: ');

z_source = input('Choose source depth: ');
z_receiver = input('Choose receiver depth: ');

N_angle=input('Number of rays: ');
theta_max=input('Max angle: ');

[R_b Z_b bottom] = make_bottom(R_max, z_max, isloop);
```

   - `make_bottom()` lets the user choose from a number of pre-made topographies.

3. `Plane_ray_2.m`

   `Plane_ray_2.m` is where the ray tracing is computed. The input in this file is only the phone spacing, which is normally set to 5 meters.

```
phone_spacing = input('Choose phone spacing: ');
```

4. `Plane_ray_3.m`

   `Plane_ray_3.m` needs no input parameters, it computes the time responses from the eigenrays.

5. `Plot_time_response.m`

   `Plot_time_response.m` is the file that plots the seismograms. It needs to be run seperately from the command line. When you run it, it will give you a list of all the cases that have been saved on the disc. Select the case you want and select source-receiver offset and resolution.

```
select = input('Select Case: ');

source_receiver = input('Select desired ...
        source-receiver offset (m): ');

resolution = input('Select desired resolution (m): ');
```

6. `Plot_eigen_ray.m`

   `Plot_eigen_ray.m` simply plots the eigenrays at a input distance.

```
receiver_range=input('Range for eigenray calculations = ');
```